PHYSICAL REVIEW B VOLUME 36, NUMBER 2 15 JULY 1987-I

# Bonding and ionicity in semiconductors

N. E. Christensen, S. Satpathy, and Z. Pawlowska*
*Max-Planck-Institut für Festkörperforschung, Postfach 80 06 65, D-7000 Stuttgart 80, Federal Republic of Germany*
(Received 4 August 1986)

Theoretical investigations of the bonding properties of 34 elemental and compound semiconductors are reported. From self-consistent band-structure calculations (within the local-density approximation) valence charge densities are calculated. The densities are obtained by transforming muffin-tin orbitals to a localized basis. Using another representation, an orthogonal basis, we construct $sp^3$ hybrids and project out the bond and antibond characters, i.e., we derive first-principles values for $sp^3$ bond orders. These, together with the first-principles tight-binding parameters, are used to study chemical trends. Relations to Phillips ionicity ($f_i$) scale are established and it is demonstrated, for example, that the critical ionicity value $f_i = 0.786$ found empirically separating the fourfold- from the sixfold-coordinated crystal structures also follows from total-energy calculations.

## I. INTRODUCTION

The group of binary $A^N B^{8-N}$ compounds with a total of eight valence electrons encompasses some of the technologically most important materials, the tetrahedrally bonded compound semiconductors. Also, these materials belong to those which have been most widely studied in experimental as well as theoretical solid-state physics.[1,2] Systematic theoretical studies of the electronic structures, optical properties, and charge distributions have been reported previously; see, for example, Refs. 3 and 4. The electron densities derived from pseudopotential calculations (e.g., Ref. 3) have been very useful for the understanding of the chemical bonds. Also we shall here present results of density calculations allowing a comparison of details in the electron distributions in several compounds. The validity of the calculations is not restricted to any particular region in space. The self-consistent band structures are calculated by means of the (relativistic) linear muffin-tin-orbital (LMTO) method. The basis is changed to the most localized orbitals providing a convenient computational scheme for obtaining the nonspherical charge densities.[5,6]

A particular aim of the present work is to discuss, quantitatively, the structural phase stability of the $A^N B^{8-N}$ compounds. The separation between crystal structures with coordination number $(N_C)=4$ and those with $N_C=6$ is determined by the competition between the covalent $sp^3$ bonding and the electrostatic interaction, which in its simplest form can be represented as an ionic Madelung interaction.

It was one of the successes of the dielectric theory derived by Phillips and van Vechten[1] that it made it possible to ascribe, in a systematic manner, an ionicity value, $f_i$, to each compound, and that a specific critical value $f_i^c = 0.786$ provided a complete separation between $N_C=4$ and $N_C=6$ structures. This relates of course to the picture of the crystal structure stabilization mentioned above, and follows also clearly from the analysis of the pressure-induced structural phase transitions in ZnTe and CdTe (Ref. 7) from the zinc-blende structure ($B3$, $N_C=4$) to the rocksalt structure ($B1$, $N_C=6$) in terms of the "frozen potential" method.[8,9] Futher, the *ab initio* calculations presented recently by Chelikowsky and Burdett[10] demonstrate this mechanism of the compositional $N_C=4 \rightarrow N_C=6$ transition. They[10] performed self-consistent calculations but used model potentials which were derived from a realistic GaAs potential but where external additional potentials were added on the anion and cation sites. In this way the ionicity was gradually changed, and from the theoretical charge transfers[11] a mapping on Phillips $f_i$ scale was obtained. A semiquantitative phase diagram was deduced, and it was shown that these first-principles calculations also lead to a critical ionicity close to 0.8.

The crystal structure stability analysis presented here differs from that of Chelikowsky and Burdett in the sense that we do not use a "controlled" potential model. Rather, we draw our conclusions by examining trends in results obtained for a large number of real compounds. These include row-1, -2, -3, and -4, IV-IV, III-V, and II-VI compounds as well as some "cross-row" compounds such as InAs, SiC, AlAs, AlSb, InP, and GaSb. Also we include one I-VII semiconductor, CuBr, although the bonding properties of the copper halides are somewhat different due to the strong admixture of the Cu $3d$ and halogen $p$ states.

The presentation of the results is organized as follows. The calculated charge-density distributions are for representative compounds shown in Sec. II. The calculation of $sp^3$ bond orders and the discussion of chemical trends follow in Sec. III. This also includes trends in calculated ionicities, metallicity values, polarities, and optical deformation potentials. The results of total-energy calculations are given in Sec. IV, and Sec. V contains a summary.

## II. CHARGE-DENSITY CALCULATIONS

As mentioned in the Introduction, charge-density calculations have been reported earlier for several compound semiconductors. Experimentally, however, only recently reliable determinations of charge distributions have been performed, and one reason for presenting density contours

 

in this work is that the validity of our calculations in principle is not restricted in space. We thus believe that they will prove valuable for future experimental work in this field.

Going outwards in a row from the homopolar semiconductors, i.e., studying the sequence of IV-IV, III-V, II-VI, to I-VII compounds, the ionicity increases. This well-known trend also follows from the quantitative density calculations, shown in Fig. 1 for row-3 compounds. The bond charge maximum, which in Ge is located halfway between the atoms, moves gradually towards the anion site (As,Se,Br). The large differences in charge density near the cation sites in (GaAs,Ge), on one hand, and (CuBr,ZnSe), on the other, is simply due to the fact that the charge-density shown for the latter two compounds includes the cation $3d$ states. This is not the case for Ge and GaAs. The self-consistent potential, however, for GaAs was calculated by allowing the Ga $3d$ to relax as valence states. The LMTO calculations involved two energy panels.[12]

Similar trends are found for the other rows, and we show in the following figures the densities in a (110) plane for rows 1, 2, 3, and 4. The first-row compounds differ somewhat from the others due to the absence of $p$ electrons in the core. Thus in diamond, for example, there is no orthogonality requirement that causes the valence $p$ states to be expelled from the region close to the atomic sites. Consequently, the density does not exhibit a maximum but rather a saddle point at the bond center [Fig. 2(a)].

Figure 2(b) shows the density in BN, and it would suggest that this compound has a large ionic bonding component. A comparison to the density calculated for GaAs [Figs. 1 and 2(b)] shows that an ionicity somewhat larger than that of GaAs ($f_i=0.321$, Ref. 1) should presumably be ascribed to BN. The value of Phillips[1] ionicity for BN ($f_i=0.256$), however, is smaller. We shall return to this point in the subsequent section where the calculated polarities and ionicities are discussed. The II-VI compound of row 1, BeO, is characterized by being very ionic as follows from Fig. 2(c).

The calculated densities for the second-row compounds, Si, AlP, and MgS are shown in Figs. 2(d), 2(e), and 2(f). The constituent atoms in this row have $2p$ states in the core, and the effect of the orthogonality of the valence $p$ states ($3p$) to these core states can be seen, for example, in the electron distributions in AlP [Fig. 2(e)]. Although we cannot[11] quantitatively derive a value of the ionicity directly from the electron density, we would expect that AlP should, in that respect, be quite similar to BN [Fig. 2(b)], maybe even slightly less ionic. MgS [Fig. 2(f)] is clearly ionic, and in fact the value[1] of $f_i$ (0.786) of this compound is just on the borderline[1] separating the fourfold- and sixfold-coordinated structures.

The electronic properties of the components in the third row are influenced by the $3d$ states. These are only in germanium lying so low in energy (binding energy $\approx 30$ eV) that their influence on the bonding properties is negligible. Already in GaAs, however, the Ga $3d$ states have moved so far up that they, via hybridization with the states at the valence band top, affect[12] the gap. In ZnSe and Zn $3d$ band is, although still rather narrow, so high lying that it clearly influences the bonding, and finally in CuBr the valence bands consist of very strongly hybridized Cu $3d$ and Br $4p$ states. The $d$-$p$ interaction produces a large hybridization gap in the halide $p$ bands of the copper halides, and these compounds are, to a large extent to be considered as $p$-$d$ bonded. Thus, it is not surprising that CuBr, CuCl, and CuI do not always fit into the trends usually expected for $sp^3$ bonded semiconductors. Details of the effects of the $d$-$p$ hybridization in the copper halides may be found in Ref. 13 and references given therein. The electron densities in Ge, GaAs, and ZnSe are shown in Figs. 2(g), 2(h), and 2(i), whereas the distribution in CuBr is shown separately in Fig. 3(c) (later).

In Figs. 2(g) and 2(h) the covalent bond charges are clearly seen—compare also to Fig. 1. In Fig. 2(i) (ZnSe) this feature is less clearly distinguished.

The charge distribution [Fig. 2(i)] in ZnSe is close to what one would expect to obtain simply from (partly) overlapping almost spherically symmetric ionic distributions. This does not imply however, that $sp^3$ bonding is unimportant in ZnSe, but the ionic contribution to the bonding must obviously be very large. This is also expressed in terms of its high value[1] (0.630) of Phillips ionicity.

We mention that in the case of GaAs we compared our calculated density to that obtained by means of the norm-conserving, relativistic and self-consistent pseudopotential theory.[14,15] The shapes of the contours obtained in this way were quite similar to those of Fig. 2(h) except for the regions close to the atomic sites. There the pseudodensity, by nature, cannot represent the electron distribution properly. But as far as the bond charged distribution is concerned, the two types of calculations give similar results.

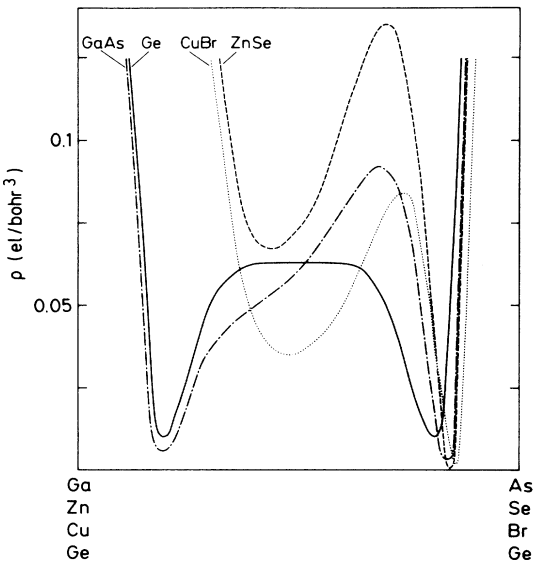


FIG. 1. Calculated density of the valence electrons along the bond direction in Ge, GaAs, ZnSe, and CuBr. The $3d$-core-like states are not included in the cases of Ge and GaAs.

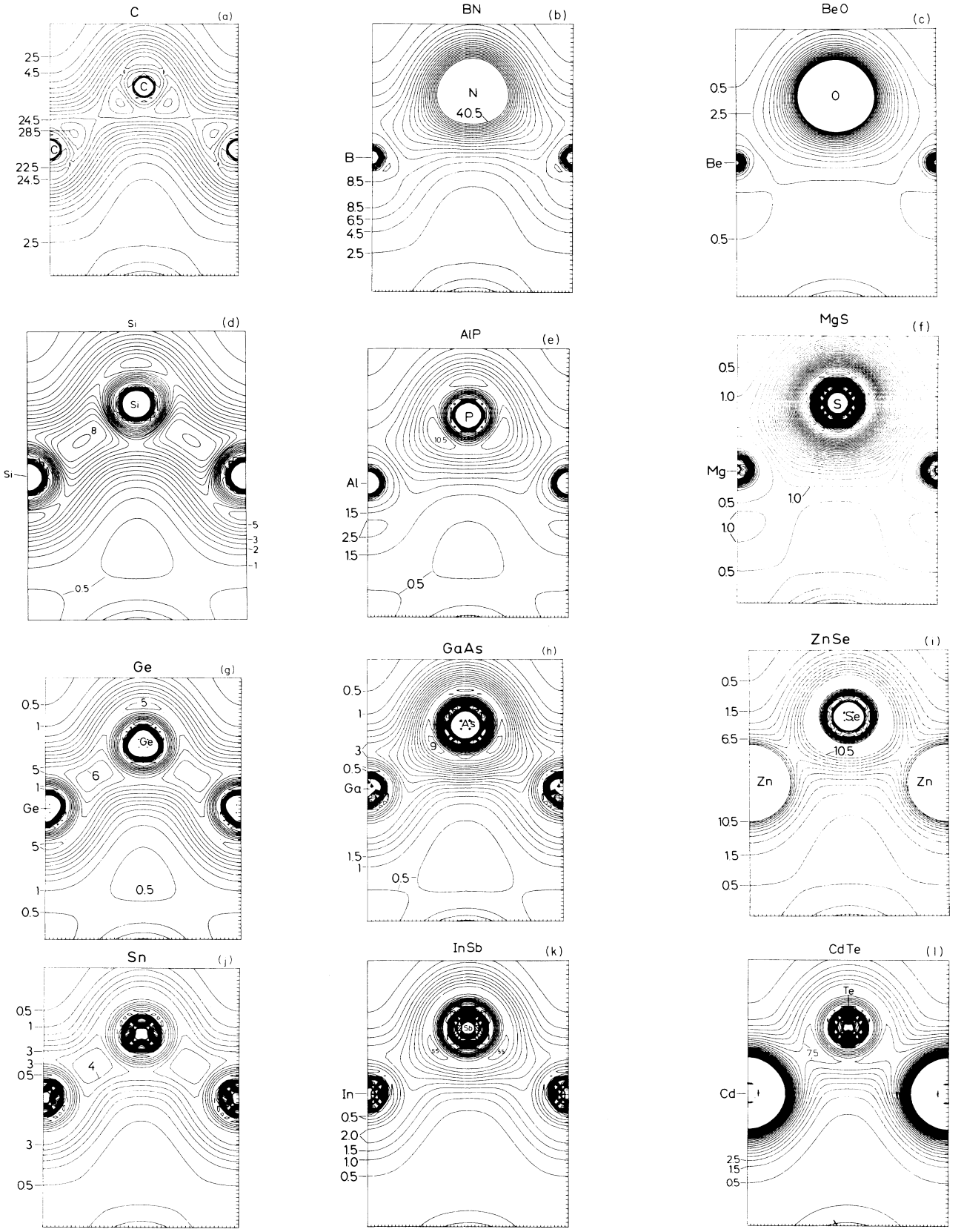


FIG. 2. Contour plot of the valence electron density in the (110) plane in row-1, -2, -3, and -4 semiconductors. The numbers on the contours give the density in units of $10^{-2}$ electrons/bohr$^3$.

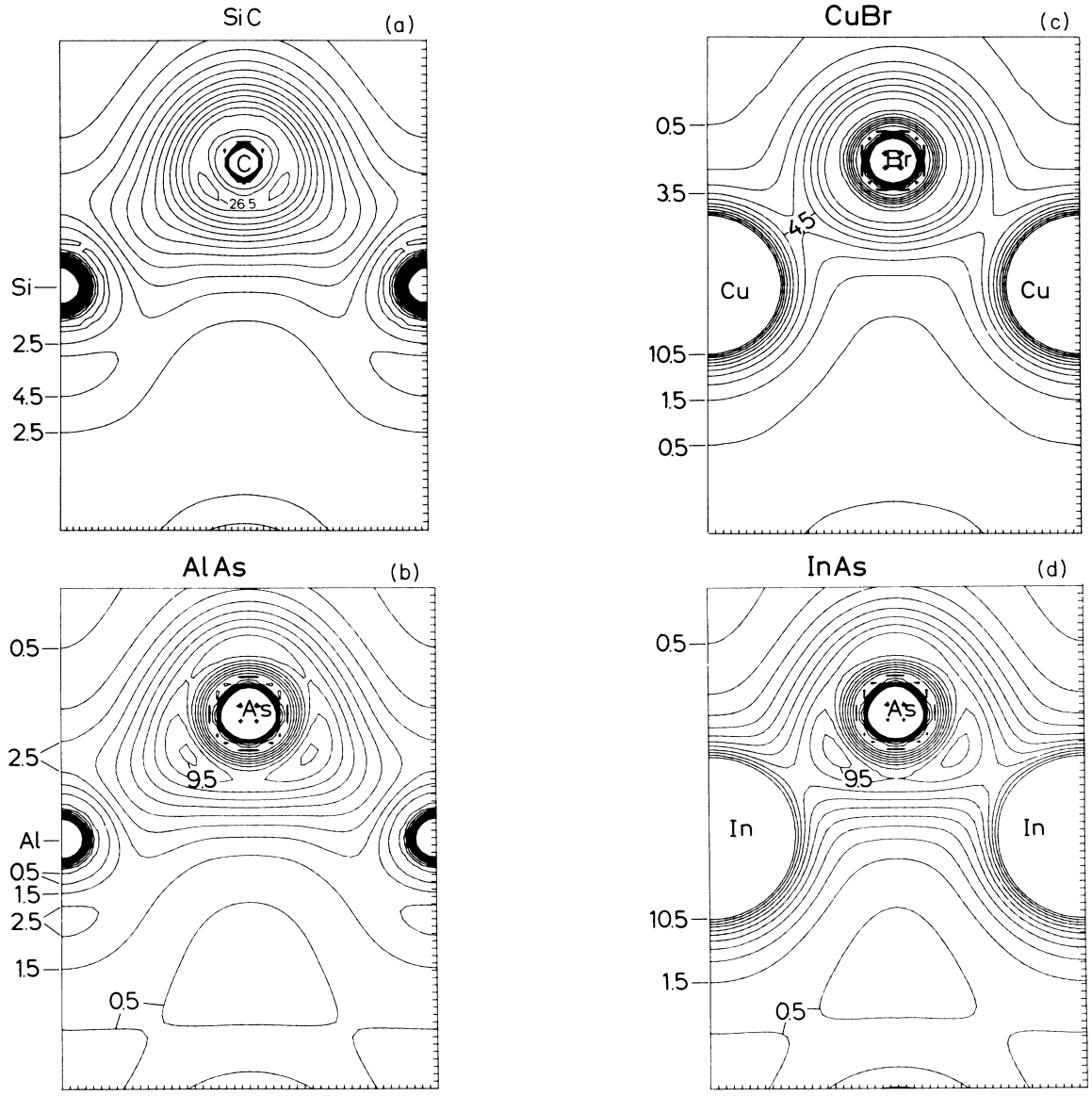


FIG. 3. (a) SiC density contours. (b) AlAs density contours. (c) CuBr density contours. (d) InAs density contours (including the In 4*d* states). (Density units as in Fig. 2.)

When passing down through the rows in the Periodic Table, the metallicity (to be defined more clearly later) of the tetrahedrally bonded compounds increases—and the gap between occupied and empty states decreases. In the fourth row, metallization of the homopolar "compound" (Sn) has occurred—the $\Gamma_2'$ state in $\alpha$-Sn lies below the top of the $p$ bands ($\Gamma_{25}'$). Although Sn is a metal, it still is characterized by strong $sp^3$ covalent bonding, and it assumes at ambient conditions the diamond crystal structure ($\alpha$-Sn). The covalency of the bonding in $\alpha$-Sn also follows from the density calculations [Fig. 2(j)]. The maximum of the bond charge density, however, is clearly lower than in Ge [Figs. 1 and 2(g)].

With increasing ionicity, i.e., going to the III-V and II-VI compounds of the fourth row, InSb and CdTe, the gap opens. The electron distribution in InSb [Fig. 2(k)] shows similarities to that of GaAs [Fig. 2(h)], and we would expect the ionicities of these compounds to be similar. Indeed, they are; $f_i$(GaAs)=0.310 and $f_i$=(InSb)=0.321 (Ref. 1). Also our bond-order calculations will support this (see the next section). The density shown for CdTe includes the contribution from the Cd 4*d* states [Fig. 2(l)].

The density contours of SiC, AlAs, CuBr, and InAs are shown in Fig. 3. The III-V compounds AlAs and InAs are examples of cross-row compounds. Apart from the large contribution from the In 4*d* states both electron distributions have great similarities with that of GaAs [Fig. 2(h)]. In spite of this similarity, Figs. 3(b), 2(h), and 3(d) clearly show the trend of increasing ionicity with increasing cation row number for a certain choice of anion constituent.

We found it interesting to include in this study the IV-IV compound SiC since its bonding properties exhibit some anomalies. According to the Phillips scale it has a

low $f_i$ value, 0.177. This is surprisingly small when the trends in ionicity are compared to those of the transverse charge (Table 9-4 in Ref. 2), from which we would expect SiC to be considerably more ionic than indicated by the value $f_i=0.177$. Indeed the density calculation, illustrated by Fig. 3(a), shows that a large fraction of the valence electrons are accumulated in the vicinity of the carbon atom. This charge flow is possible because C has no $p$ states in the core, i.e., there are no orthogonality requirements that would prevent the valence $p$ states to accumulate near the nucleus. Thus electrons easily flow from Si to C, and the compound gets a large ionicity. A similar conclusion was reached by Churcher *et al.*,[16] who from their calculated pseudodensity suggest that SiC should have an ionicity comparable to that of ZnS. Also, this would agree[16] with the similar $r_\sigma$ parameters[17] of SiC and ZnS.

## III. IONICITIES AND BOND ORDERS: CHEMICAL TRENDS

In this section the calculation of $sp^3$-bond orders, metallicities ($\alpha_m$), polarities ($\alpha_p$) and ionicities ($f_i$) are described. This requires two different types of calculations. The quantities $\alpha_m$, $\alpha_p$, and $f_i$ will be defined in analogy with those given in Refs. 1 and 2, and their evaluation thus requires the construction of a transformation to a formal $sp^3$ tight-binding Hamiltonian of the size $8\times 8$. This transformation is only approximate, but sufficiently accurate for the study of chemical trends in $\alpha_m$, $\alpha_p$, and $f_i$. Our method differs from that of Ref. 2 by allowing us to deduce these quantities directly from potential parameters derived from the first-principles LMTO calculations. Also, this means that we can study the variation of them with, for example, pressure.

For the purpose of calculating the bond orders, $sp^3$ bonding and antibonding contributions, we use another formulation of the LMTO, or rather another representation, namely, the (nearly) orthogonal representation.

Section III is divided into three parts: III A, III B, and III C. Section III A contains the essentials of the formalism needed for the transformations and necessary to establish the connection to $f_i$, $\alpha_m$, and $\alpha_p$. Section III B contains the explicit expressions of these quantities in terms of the potential parameters, and the numerical results are collected in Sec. III C.

### A. LMTO: Choices of representation

Details of the LMTO formalism which we use may be found in Refs. 18, 19, and 5, and 20–22. In order to define the terminology and to introduce the relevant parameters we shall, however, describe here how we choose the proper representations.

The wave function corresponding to a state $j$ may, in a representation "$\alpha$" (see below), be expressed as

$$\Psi_j(\mathbf{r})=\sum_{R,L} |\chi^\alpha(\mathbf{r}_R)\rangle_{RL}^{\infty} u^\alpha_{RL,j} \equiv |\chi^\alpha\rangle\cdot\mathbf{u}^\alpha_j , \tag{1}$$

where the index $R$ refers to the position vector $\mathbf{R}$ of an atomic site (real-atom or "empty-sphere" site), $L\equiv(l,m)$ is combined angular-momentum index, and $u$ is the eigenvector. The basis functions $\chi$ are of the form[19,5,6,20,21]

$$\chi^\alpha_{RL}(\mathbf{r}_R)=\phi_{RL}(\mathbf{r}_R)+\sum_{R',L'}\dot\phi^{\,\alpha}_{R'L'}(\mathbf{r}_{R'})h^\alpha_{R'L',RL}+\chi^{\alpha,\dot l}_{RL}(\mathbf{r}_R) . \tag{2}$$

The last term in Eq. (2) is, for example, specified in Eq. (6) of Ref. 6. The function $\phi_{rL}(\mathbf{r}_R)$ is a product of a spherical harmonic and the solution $\phi_{vRl}(|\mathbf{r}_R|)$ to the radial wave equation inside a sphere centered at the position $\mathbf{R}$ and corresponding to a certain energy $E_{vRl}$. The functions $\dot\phi^{\,\alpha}$ are linear combinations of the $\phi$ functions and their energy derivatives $\dot\phi$. The label "$\alpha$" specifies the choice of this linear combination, i.e., the representation. The matrix $\underline{h}^\alpha$ is

$$\underline{h}^\alpha=\underline{c}^\alpha-\underline{E}_v+(\underline{\Delta}^\alpha)^{1/2}\underline{S}^\alpha(\underline{\Delta}^\alpha)^{1/2} , \tag{3}$$

where the structure constants in the $\alpha$ representation are given through

$$\underline{S}^\alpha=\underline{S}^0(\underline{1}-\underline{\alpha}\,\underline{S}^0)^{-1} \tag{4}$$

in terms of the conventional[18,19,5] structure constants $S^0$. The diagonal matrix $\underline{\alpha}$ contains the parameters specifying the screening chosen. The choice $\alpha=0$ corresponds to the conventional LMTO as described in Ref. 18. This is also the formalism which is used by Skriver,[22] and which is implemented in his computer codes.[22] The diagonal matrices $\underline{c}^\alpha$ and $\underline{\Delta}^\alpha$ contain potential parameters which determine, within the linearization scheme, the potential functions $\underline{P}^\alpha(E)$. In the conventional representation ($\alpha=0$), the parameters $c=C_{Rl}$ ($l$ indicating the angular momentum), and $\Delta=\Delta_{Rl}$ are the bond-center and bandwidth parameters. $C_{Rl}$ is the energy[18,22] for which the logarithmic derivative of the radial wave function, at $r=s$ (the atomic sphere radius) equals $-l-1$. The parameter $\Delta$ is given by

$$\Delta=\frac{1}{2}\left[\frac{s}{w}\right]^{2l+1}[s\Phi_-^2]_{R,l} , \tag{5}$$

where $w$ is the (average) Wigner-Seitz radius, i.e., the radius of (overlapping) space-filling spheres of equal size. The quantity $\Phi_-$, and a similar $\Phi_+$, are (omitting indices $R$ and $l$)

$$\begin{aligned}\Phi_+&=\phi_v+\omega_+\dot\phi_v ,\\ \Phi_-&=\phi_v+\omega_-\dot\phi_v ,\end{aligned} \tag{6}$$

in terms[18] of the radial wave function $\phi_v$ and its energy derivative evaluated at $r=s$. The coefficients $\omega_+$ and $\omega_-$ are $\omega(l)$ and $\omega(-l-1)$ with $\omega(D)$ as defined in Eq. 3.45 of Ref. 22. The inverse of the potential function $P$, referred to above, is, in terms of the parameters $\Delta$ and $C$,

$$P(E)^{-1}=\frac{\Delta}{E-C}+\gamma , \tag{7}$$

where[18,22]

$$\gamma=\gamma_{Rl}=\frac{1}{2(2l+1)}\left[\frac{s}{w}\right]^{2l+1}\left[\frac{\Phi_-}{\Phi_+}\right]_{R,l} . \tag{8}$$

Relations between $P(E)$ and the logarithmic derivatives $D(E)$ are given in Refs. 18 and 22:

$$P(E)=2(2l+1)\left[\frac{D(E)+l+1}{D(E)-l}\right]_{R,l} . \quad (9)$$

From these functions, the band structure may be obtained using the bare, structure-constant matrices in $\mathbf{k}$ space, $S_{L,L}(\mathbf{k})$, from the[18,22] atomic-sphere-approximation Korringa-Kohn-Rostoker (ASA-KKR) equations:

$$\det[P_l(E)\delta_{L'L}-S_{L'L}(\mathbf{k})]=0 . \quad (10)$$

In an arbitrary representation $\alpha$, we have[19,5,20,21]

$$[P^{\alpha}(E)]^{-1}+\alpha=[P(E)]^{-1} . \quad (11)$$

Apart from the choice of representation already mentioned ($\alpha=0$) there are two others of particular importance. The values[20]

$$\alpha_l=\begin{cases}0.348\,50, & l=0\\ 0.053\,03, & l=1\\ 0.010\,714, & l=2\end{cases} \quad (12)$$

correspond to the case with maximum screening. In this version the LMTO is transformed into a first-principles tight-binding (TB) scheme. This representation is the one which is most convenient for the calculation of the charge distributions[5,6] due to the strong localization of the orbitals. To lowest order, the Hamiltonian is

$$\underline{H}^{(1)}=\underline{c}^{\alpha}+\underline{\Delta}^{\alpha(1/2)}\underline{S}^{\alpha}\underline{\Delta}^{\alpha(1/2)}=\underline{h}^{\alpha}+\underline{E}_{\nu} \quad (13)$$

or, in the notation of Ref. 20,

$$\overline{H}^{(1)}=\overline{C}+\overline{\Delta}^{1/2}\overline{S}\,\overline{\Delta}^{1/2} . \quad (13a)$$

The real-space structure constants are given, for this scheme in Table I of Ref. 20. The values of $c^{\alpha}$ and $\Delta^{\alpha}$($\overline{C}$ and $\overline{\Delta}$) in the tight-binding scheme are given by

$$c^{\alpha}=E_{\nu}+\omega_{-}^{\alpha} , \quad (14)$$

with

$$\omega_{-}^{\alpha}=\left[1+(\alpha-\gamma)\frac{\omega_{-}}{\Delta}\right]\omega_{-} , \quad (15)$$

$$\Delta^{\alpha}=\Delta\left[1+(\alpha-\gamma)\frac{\omega_{-}}{\Delta}\right]^{2} . \quad (16)$$

The structure constants which we use here for the zinc-blende-type semiconductors are those given in Table I (Ref. 20) for the bcc lattice since we include the "empty spheres." In the following we shall use an overbar (e.g., $\overline{\Delta}$) to indicate that (13)–(16) are evaluated with (12).

The localized representation (12) will later be used to estimate cation and anion $s$ and $p$ energy levels ($E_{s,p}^{c,a}$), $sp^3$-hybrid energies ($E_{sp^3}^{c,a}$) and $sp^3$–bond-antibond hybrid levels. For this purpose we neglect the empty spheres, and we further approximate the overlap matrix by a unit diagonal matrix. If we then further neglect the $d$ states on the atomic sites, the Hamiltonian [Eq. (13)] is formally equivalent to the ($s,p_x,p_y,p_z$) $8\times8$ tight-binding Hamiltonian as used, for example, by Harrison (Ref. 2). This is convenient for the study of chemical trends in ionicity, metallicity, etc., and with a small modification to be described below, the method is sufficiently accurate for this purpose. A more accurate, and from a theoretical point of view more appealing, method would consist in folding the empty-site $p$ and $d$ states and the real-atom $d$ states down[20] by a procedure related to that described in Ref. 21. The matrices are then $10\times10$, and correspond roughly to a first principles version of the $sp^3s^*$ model.[21,23] Such a full down folding would, however, produce a partial unscreening and may therefore not be very adequate[24] when we wish to use a localized basis. We use, for the purposes mentioned above, the Hamiltonian in Eq. (13a), but with $\overline{S}$ slightly modified. This change consists in formal down folding[24] of the $d$ states on the real atomic sites. This is done by replacing $\overline{S}=\overline{S}^{LL}$ [$L$ here means $s$ and $p$ states, $H$ means $d$-states (higher $l$ states)] by

$$\overline{\overline{S}}^{LL}=\underline{\overline{S}}^{LL}+\underline{\overline{S}}^{LH}\underline{\overline{F}}^{HH}(E_H)\underline{\overline{S}}^{HL} , \quad (17)$$

with

$$\overline{F}^{HH}=(\underline{\overline{P}}^{H}-\underline{\overline{S}}^{HH})^{-1} , \quad (18)$$

where $\underline{\overline{P}}^{H}$ is the diagonal potential-function matrix given by the second-order[20] matrix expression

$$\underline{\overline{P}}^{H}(E_H)=\left[\left[\frac{\Delta_d}{E_H-C_d}+\gamma_d-\alpha_d\right]^{-1}\right] . \quad (19)$$

For the energy $E_H$ we use

$$E_H=C_d+\frac{\Delta_d}{P_d^{-1}-\gamma_d} , \quad (20)$$

with $P_d^{-1}$ set equal to zero. Thus $E_H$ here is taken to be the "square-well pseudopotential," $V_d$ (see for example Ref. 18). With this choice $\underline{\overline{P}}^{H}=-\underline{\alpha}_d^{-1}$.

We shall not use this scheme for accurate band-structure calculations. For that purpose we apply the full LMTO or its exact transformation into a tight-binding formalism with 36 basis functions. Nevertheless, in order to justify our application of the scheme for the purposes mentioned, we compare, for Si, in Table I the crude estimates of eigenvalues at $\Gamma$ obtained from the $8\times8$ Hamiltonian (13) and (17) to full LMTO calculations. All calculations were based on the same potential.

The first column of Table I contains the "correct" LDA (local-density approximation) eigenvalues obtained from a self-consistent LMTO calculation with $s$, $p$, and $d$ partial waves on the Si sites as well as on the empty-sphere sites ($E$). Further, the "combined correction term" is included in this case ($a$). This corrects[18] for the nonspherical shape of the cells *and* for the truncation of higher partial waves. The lowest row in Table I gives the calculated values of the $p$-$s$ gap, $E(\Gamma_2')-E(\Gamma_{25}')$, and it is seen, as demonstrated elsewhere,[25,12] that this correction is very important if accurate band-gap values are required. This becomes, of course, much more pronounced if the number of partial waves is further reduced as in the calculations illustrated by columns $c$ and $d$. With a cutoff at $l_{\max}=1$ on all sites the combined correction term shifts the $\Gamma_{25}'$ level (valence-band top) by $\sim1.35$ eV. The last two columns in Table I give the crude tight-binding ener-

TABLE I. Si: Eigenvalues and $p \rightarrow s$ gap at $\Gamma$ in eV. Scalar-relativistic LMTO calculations including "empty spheres" are given. In all cases the same potential (self-consistent with specifications as in column *a*) was used. The same maximum $l$ was used on real-atomic sites and those of the empty spheres. *a* indicates *s*, *p*, and *d*, combined correction term included. *b* indicates *s*, *p*, and *d* no combined correction term. *c* indicates *s* and *p*, combined correction term inclued. *d* indicates *s* and *p*, without combined correction term. *e* indicates *s* and *p*, crude $8\times8$ formal tight binding. *f* indicates *s* and *p*, formal $8\times8$ tight binding with Si *d* states "folded down."

| | *a* | *b* | *c* | *d* | *e* | *f* |
|---|---|---|---|---|---|---|
| $\Gamma_2'(c)$ | 2.161 | 2.820 | 2.051 | 2.823 | 1.539 | 2.826 |
| $\Gamma_{15}(c)$ | 1.813 | 1.539 | 2.825 | 5.808 | 7.223 | 8.338 |
| $\Gamma_{25}'(v)$ | −0.868 | −1.046 | −0.120 | 1.225 | 1.277 | 0.161 |
| $\Gamma_1(v)$ | −12.92 | −12.93 | −12.91 | −12.92 | −10.22 | −11.51 |
| $\Gamma_2'-\Gamma_{25}'$ | 3.029 | 3.866 | 2.171 | 1.598 | 0.262 | 2.665 |

gy levels obtained from (13) and (17). Clearly, without the down folding (column *e*) the *p-s* gap is very much in error, 0.26 eV as compared to the "correct" value 3.03 eV (*a*). This kind of calculation would thus, for Si, lead to a by far too large value of the metallicity. The simplified down folding, however, improves the results considerably. The value of the valence-band top in column *f* has dropped by $\sim 1.1$ eV as compared to the value in *e*, i.e., this result does not differ very much from the calculation with *s* and *p* basis function *and* the inclusion of the combined correction term (column *c*). In general, i.e., for a large number of zinc-blende-type compounds, we find that the energy levels [$\Gamma_1^v$, $\Gamma_{15}^v$, and $\Gamma_1^c$, or $\Gamma_1(v)$, $\Gamma_{25}'(v)$, and $\Gamma_2'(c)$ in the homopolar semiconductors] systematically are 0.5–0.8 eV too high in energy when estimated from the type of calculation used in column *f* of Table I. This is illustrated in Figs. 4 and 5, where we have plotted the estimated $\Gamma_{15}^v$ and $\Gamma_1^c$ levels versus those calculated using the full LMTO method with combined correction term. Note that in Fig. 5 we plot $\Gamma_1^c$ relative to the valence-band top ($\Gamma_{15}^v$), i.e., we have shown the $E_0$ gap (not always the "true" gap, cf. Si and Ge). The energies in Fig. 4, on the other hand, are measured with respect to the natural reference level in the LMTO; namely, the potential at infinity of a single atomic sphere. In our TB scheme we "automatically" get the energies on that scale. This is important to keep in mind when our TB scheme is compared to that of Harrison, where the diagonal matrix elements are taken from free-atom calculations, i.e, they are volume independent.

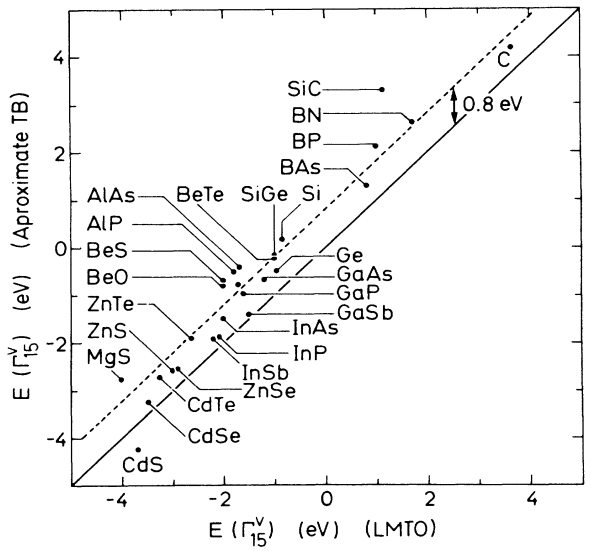


FIG. 4. Valence-band edges ($\Gamma_{15}^v$) as estimated from our formal $8\times8$ ($s,p_x,p_y,p_z$) tight-binding Hamiltonian versus the "correct" values (i.e., calculation as column *a* in Table I). (Energies are given in eV on the natural LMTO scale on which the reference level is the potential at infinity from a single atomic sphere.)

The calculation of the bond orders, i.e., bonding-antibonding contributions to the occupied states in the diamond-type crystals, require a different kind of scheme. The values obtained depend on which type of basis is used. If, for example, we had chosen a basis consisting of bond-centered Wannier functions,[26] we would get 100% bonding for the tetrahedral bond for all the semiconductors. Thus, in this way we would not learn anything about chemical trends in the bonding characteristics. In our conventional LMTO calculation we project out the *s*, *p*, and *d* occupancies ($n_{R,l}$) at each site: *A*, (0,0,0); *B*, (1,1,1)*a*/4; *C*, (1,1,1)*a*/2; and *D*, (−1,−1,−1)*a*/4. Here *A* and *B* are occupied by real atoms and *C* and *D* are the empty-sphere positions. In the construction of $sp^3$ hy-

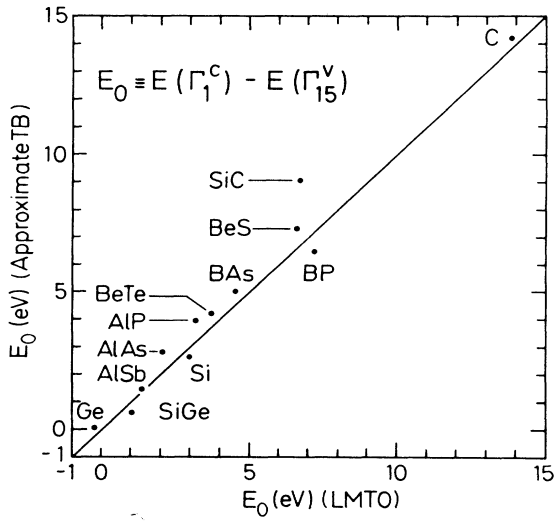


FIG. 5. Direct $p \rightarrow s$ gaps ($\Gamma_1^c - \Gamma_{15}^v$) as given by the $8\times8$ Hamiltonian vs the full LMTO results.

brids for the $A-B$ bond we wish to use $n_{A,s}$, $n_{A,p}$, $n_{B,s}$, and $n_{B,p}$ without changing their values. For this reason we use the LMTO method with the *orthogonal* basis. This is done[19,20] by choosing $\alpha_{Rl}=\gamma_{Rl}$ [Eq. (8)]. For the atoms $A$ and $B$ we combine the $s$ and $p$ orbitals to form the $sp^3$ hybrids [$\frac{1}{2}(s+p_x+p_y+p_z)$, etc.] Then the $sp^3$ hybrids on neighboring sites are combined to form $sp^3$-hybridized bond and antibond orbitals. Thus a new basis set is formed; it consists of four bond orbitals, four antibond orbitals, ten $d$ orbitals on the sites $A$ and $B$, and 18 empty-sphere orbitals ($C$ and $D$). The latter 28 orbitals are unmodified. In this basis we calculate the eigenvectors. The components of the eigenvector for band $n$ with wave vector $\mathbf{k}$ corresponding to the bond orbitals are called $b_i^{n\mathbf{k}}$, and those referring to the antibond orbitals $a_j^{n\mathbf{k}}$ ($j=1,2,3,4$). The total bond character $\mathcal{B}$ is obtained by integrating over the Brillouin zone

$$\mathcal{B}=\tfrac{1}{2}\sum_{\mathbf{k}\in \mathrm{BZ}}\left[\sum_{n=1}^{4}\sum_{j=1}^{4}|b_j^{n\mathbf{k}}|^2\right] . \tag{21}$$

From the coefficients $a_j^{n\mathbf{k}}$, the antibonding character, $\mathcal{A}$, is calculated in the same way. The bond order $b$ for the tetrahedral bond between the two ("real") atoms in the compound is

$$b=\mathcal{B}-\mathcal{A} . \tag{22}$$

### B. Definition of ionicity metallicity, and polarity

The preceding subsection describes how the bond orders are calculated in the orthogonal representation, and how the TB formulation is used to construct a formal $8\times 8$ tight-binding Hamiltonian. This is the one which we use in estimates of metallicities, etc., from the first-principles potential parameters. The matrix elements of this Hamiltonian in the basis of cation ($c$) and anion ($a$) $s$ and $p$ states are as follows. Diagonal:

$$E_s^a=\langle s^a|H|s^a\rangle=\bar{C}_s^a+\bar{\Delta}_s^a\bar{S}_s^{\mathrm{on}} , \tag{23}$$

$$E_p^a=\langle p_x^a|H|p_x^a\rangle=\bar{C}_p^a+\bar{\Delta}_p^a\bar{S}_p^{\mathrm{on}} , \tag{24}$$

and similarly for $E_s^c$ and $E_p^c$. Off diagonal (in the notation of Pötz and Vogl[27]):

$$V_{ss}=4(\bar{\Delta}_s^a)^{1/2}S_{ss}(\bar{\Delta}_s^c)^{1/2} , \tag{25}$$

$$V_{xx}=4(\bar{\Delta}_p^a)^{1/2}S_{xx}(\bar{\Delta}_p^c)^{1/2} , \tag{26}$$

$$V_{sx}=4(\bar{\Delta}_s^a)^{1/2}S_{sx}(\bar{\Delta}_p^c)^{1/2} , \tag{27}$$

$$V_{xs}=4(\bar{\Delta}_p^a)^{1/2}S_{sx}(\bar{\Delta}_s^c)^{1/2} \tag{28}$$

[$V_{xx}=4E_{xx}$(Harrison), Ref. 2], and similar $xz$, $xy$, $sy$, etc., expressions. In Eqs. (23) and (24) $\bar{S}_{s,p}^{\mathrm{on}}$ are the onsite bcc screened structure constants. The structure constants in Eqs. (25)–(28) are the nearest-neighbor $s$-$s$, $p_x$-$p_x$, $s$-$p_x$ structure-constant matrix elements of $\bar{S}$ (Ref. 20) if no down folding is made, or $\bar{\bar{S}}$, Eq. (17), with $d$ down folding. The diagonal elements, $E_{s,p}^{a,c}$ [(23)–(24)], correspond formally to Harrison[2] energies $\epsilon_{s,p}^{a,c}$, but our $s$ and $p$ levels are derived from the actual crystal potential, whereas those of Ref. 2 are taken from free-atom calculations.

The $sp^3$-hybrid energy levels are

$$E_{sp^3}^{a,c}=(E_s^{a,c}+3E_p^{a,c})/4 . \tag{29}$$

The energy separation $E_G$ between $sp^3$-hybrid bond and antibond states has two components, $\Delta E_{sp^3}$ and $-2h$, where

$$\Delta E_{sp^3}=E_{sp^3}^c-E_{sp^3}^a \tag{30}$$

and $h$ is the hopping integral

$$\begin{aligned} h&=\tfrac{1}{4}\langle s^a+p_x^a+p_y^a+p_z^a|\bar{H}^{(1)}|s^c-p_x^c-p_y^c-p_z^c\rangle \\ &=\tfrac{1}{16}[V_{ss}-3V_{xx}-6V_{xy}-3(V_{sx}-V_{xs})] \end{aligned} \tag{31}$$

and

$$E_G=[(\Delta E_{sp^3})^2+(2h)^2]^{1/2} . \tag{32}$$

In a homopolar semiconductor $\Delta E_{sp^3}$ vanishes, and only the hybridization contribution, $-2h$, to $E_G$ is nonzero. The magnitude of $\Delta E_{sp^3}$, i.e., the offset of the cation and anion hybrid energy levels is a measure of the ionicity of the bond. Obviously this quantity is the component which Phillips[1] refers to as "$C$," and his "$E_h$" is equivalent to $-2h$. Thus we can in our model directly calculate the ionicity $f_i^*$ within a definition that agrees with that used by Phillips:[1]

$$f_i^*=(\Delta E_{sp^3})^2/E_G^2=\frac{(\Delta E_{sp^3})^2}{(\Delta E_{sp^3})^2+(2h)^2} . \tag{33}$$

(We use an asterisk to distinguish our calculated ionicities from the values $f_i$ on the original Phillips scale.)

The $s$-like energy levels at $\Gamma$ are, in the tight-binding scheme

$$E(\Gamma_1)=\tfrac{1}{2}(E_s^a+E_s^c)\pm[\tfrac{1}{4}(E_s^c-E_s^a)^2+V_{ss}^2]^{1/2} , \tag{34}$$

and the $p$-like status have the energies

$$E(\Gamma_{15})=\tfrac{1}{2}(E_p^a+E_p^c)\pm[\tfrac{1}{4}(E_p^a-E_p^c)^2+V_{xx}^2]^{1/2} . \tag{35}$$

These equations were used in the calculations of the energies in Table I, columns $e$ and $f$ and Figs. 4 and 5. For the homopolar semiconductors the label $\Gamma_{25}'(v)\sim\Gamma_{15}^v$ and $\Gamma_2'(c)\sim\Gamma_1^c$, but the energies are still given by (35) (minus sign) and (34) (plus sign). From Eqs. (34) and (35) we find that the gap $E_0$ between the top of the valence band ($p$) and the bottom of the $s$-like conduction band is

$$E_0=-E_0^{(1)}+E_0^{(2)} , \tag{36}$$

with

$$E_0^{(1)}=\tfrac{1}{2}(E_p^a+E_p^c)-\tfrac{1}{2}(E_s^a+E_s^c) \tag{37}$$

and

$$E_0^{(2)}=[\tfrac{1}{4}(E_s^c-E_s^a)^2+V_{ss}^2]^{1/2}+[\tfrac{1}{4}(E_p^c-E_p^a)^2+V_{xx}^2]^{1/2} . \tag{38}$$

The competition between these terms determines the gap $E_0$, and it is natural to define the *metallicity* $\alpha_m$ through

$$\alpha_m = E_0^{(1)}/E_0^{(2)} \ . \tag{39}$$

This definition is identical to Harrison's (Ref. 2, Sec. 3-E). We also calculate the *polarity* $\alpha_p$ using the definition which is similar to that of Ref. 2:

$$\alpha_p = \tfrac{1}{2}(E_p^c - E_p^a)[\tfrac{1}{4}(E_p^c - E_p^a)^2 + V_{xx}^2]^{-1/2} \ . \tag{40}$$

### C. Numerical results

This subsection contains the numerical results obtained for the bond orders ionicity parameters, etc. First, we give in Table II a listing of potential parameters $\bar{\Delta}$ as well as $s$ and $p$ levels [Eqs. (23)–(24)] $E_{s,p}^{c,a}$. Harrison's phenomenological model[2] assumes that that the $s$-$s$, $s$-$p$, and $p$-$p$ interatomic matrix elements have the form

$$V_{ll'm} = \eta \frac{\hbar^2}{m_0 d^2} \ , \tag{41}$$

where $d$ is the bond length. This $d^{-2}$ scaling is widely used, for example in calculations of deformation potentials.[27] In order to examine whether this scaling also applies to our model, we include in Table II calculated values of

$$\xi_{ll'}^{\alpha\gamma} = \frac{d \ln[(\bar{\Delta}_l^{\alpha}\bar{\Delta}_{l'}^{\gamma})^{1/2}]}{d \ln d} \ . \tag{42}$$

[The scaling in Eq. (41) corresponds to $\xi = -2.$] It follows that the interatomic matrix elements in our model scale are different from those of Harrison's model. For the $p$-$p$ elements we have typically $\xi \simeq -2.7$ and for the $s$-$s$ elements $\xi \simeq -3.0$. This does not imply that we claim that our calculations prove the volume scaling of Harrison's model to be wrong. The scaling exponents calculated from (42) in our case refer in fact to a first-principles tight-binding scheme with *36* basis functions, i.e., with $s$, $p$, and $d$ orbitals on the real-atom sites as well as on the empty-sphere sites. Further, in our TB scheme the diagonal elements, the energies $E_{s,p}^{a,c}$, are calculated from the actual crystal potential. This means that their values depend on the volume. This is not the case in Harrison's model, where these levels are taken from free-atom calculations. Thus, it is not surprising that our $\xi$ values for $s$ and $p$ orbitals differ from $-2$.

TABLE II. The potential parameters $\bar{\Delta}$ [Eqs. (12) and (16)], $s$ and $p$ levels [Eqs. (23) and (24)], and powers $\xi_{ll'}^{\alpha\gamma}$ [Eq. (42)]. $E$ and $\bar{\Delta}$ are in rydbergs.

| Compound | $\bar{\Delta}_s^c$ | $\bar{\Delta}_p^c$ | $\bar{\Delta}_s^a$ | $\bar{\Delta}_s^a$ | $E_s^c$ | $E_p^c$ | $E_s^a$ | $E_p^a$ | $\xi_{ss}$ | $\xi_{xx}$ | $\xi_{sx}$ | $\xi_{xs}$ |
|---|---|---|---|---|---|---|---|---|---|---|---|---|
| AlAs | 0.174 | 0.083 | 0.152 | 0.100 | −0.077 | 0.370 | 0.714 | 0.149 | −3.15 | −2.57 | −2.66 | −3.07 |
| AlP | 0.183 | 0.086 | 0.158 | 0.099 | −0.022 | 0.429 | 0.634 | 0.128 | −3.09 | −2.65 | −2.72 | −3.02 |
| AlSb | 0.141 | 0.072 | 0.146 | 0.092 | −0.235 | 0.220 | −0.646 | 0.125 | −3.27 | −2.69 | −2.77 | −3.18 |
| BAs | 0.208 | 0.103 | 0.256 | 0.143 | −0.064 | 0.412 | −0.392 | 0.555 | −2.92 | −2.57 | −2.58 | −2.90 |
| BN | 0.368 | 0.172 | 0.321 | 0.164 | 0.732 | 1.051 | −0.428 | 0.521 | −2.70 | −2.83 | −2.68 | −3.03 |
| BP | 0.233 | 0.114 | 0.275 | 0.150 | 0.045 | 0.514 | −0.245 | 0.575 | −2.74 | −2.54 | −2.53 | −2.75 |
| BeO | 0.308 | 0.146 | 0.209 | 0.126 | 1.138 | 1.151 | −1.068 | 0.094 | −3.52 | −2.68 | −2.34 | −3.87 |
| BeS | 0.196 | 0.090 | 0.201 | 0.126 | 0.253 | 0.467 | −0.809 | 0.122 | −2.97 | −2.76 | −2.57 | −3.15 |
| BeSe | 0.182 | 0.084 | 0.193 | 0.127 | 0.170 | 0.405 | −0.853 | 0.174 | −3.09 | −2.77 | −2.60 | −3.26 |
| BeTe | 0.156 | 0.074 | 0.195 | 0.121 | 0.041 | 0.309 | −0.691 | 0.233 | −3.14 | −2.77 | −2.62 | −3.29 |
| CuBr | 0.178 | 0.153 | 0.100 | 0.083 | 0.083 | 0.942 | −1.356 | −0.318 | −3.59 | −2.34 | −2.83 | −3.09 |
| CdS | 0.176 | 0.071 | 0.082 | 0.073 | −0.030 | 0.399 | −0.954 | −0.194 | −5.06 | −2.90 | −3.11 | −4.84 |
| CdSe | 0.160 | 0.067 | 0.076 | 0.076 | −0.089 | 0.336 | −0.989 | −0.182 | −5.23 | −3.04 | −3.26 | −5.01 |
| CdTe | 0.138 | 0.062 | 0.144 | 0.080 | −0.188 | 0.237 | −0.942 | −0.131 | −4.80 | −3.27 | −3.39 | −4.69 |
| GaAs | 0.179 | 0.090 | 0.170 | 0.097 | −0.226 | 0.395 | −0.721 | 0.140 | −3.76 | −2.88 | −3.11 | −3.52 |
| GaP | 0.199 | 0.096 | 0.181 | 0.099 | −0.186 | 0.440 | −0.654 | 0.106 | −3.49 | −2.70 | −2.93 | −3.26 |
| GaSb | 0.145 | 0.077 | 0.176 | 0.093 | −0.383 | 0.222 | −0.661 | 0.112 | −4.05 | −3.09 | −3.44 | −3.70 |
| HgPo | 0.119 | 0.054 | 0.082 | 0.074 | −0.376 | 0.150 | −1.441 | −0.154 | −4.16 | −3.10 | −3.16 | −4.11 |
| InAs | 0.164 | 0.078 | 0.113 | 0.081 | −0.252 | 0.297 | −0.828 | −0.008 | −3.54 | −2.67 | −2.92 | −3.28 |
| InP | 0.188 | 0.085 | 0.134 | 0.082 | −0.160 | 0.404 | −0.740 | −0.006 | −3.85 | −2.71 | −3.02 | −3.54 |
| InSb | 0.143 | 0.072 | 0.141 | 0.080 | −0.340 | 0.212 | −0.738 | 0.013 | −3.89 | −2.88 | −3.19 | −3.58 |
| MgS | 0.159 | 0.064 | 0.107 | 0.082 | 0.200 | 0.451 | −0.933 | −0.128 | −4.45 | −2.55 | −2.70 | −4.30 |
| SiC | 0.308 | 0.147 | 0.235 | 0.123 | 0.384 | 0.998 | −0.242 | 0.475 | −2.56 | −2.25 | −2.37 | −2.43 |
| SiGe | 0.168 | 0.094 | 0.167 | 0.096 | −0.387 | 0.236 | −0.478 | 0.273 | −3.19 | −2.65 | −2.88 | −2.96 |
| ZnPo | 0.132 | 0.113 | 0.123 | 0.094 | −0.229 | 0.510 | −1.037 | 0.019 | −3.83 | −2.17 | −2.94 | −3.05 |
| ZnS | 0.178 | 0.076 | 0.132 | 0.093 | −0.029 | 0.411 | −0.989 | −0.109 | −3.36 | −2.78 | −2.73 | −3.41 |
| ZnSe | 0.190 | 0.158 | 0.126 | 0.093 | −0.041 | 0.813 | −1.035 | −0.082 | −3.29 | −2.24 | −2.67 | −2.86 |
| ZnTe | 0.145 | 0.069 | 0.162 | 0.094 | −0.192 | 0.287 | −0.897 | −0.027 | −3.94 | −3.04 | −3.10 | −3.88 |
| C | 0.387 | 0.186 | 0.387 | 0.186 | 0.259 | 0.899 | 0.259 | 0.899 | −2.57 | −2.52 | −2.54 | −2.54 |
| Si | 0.182 | 0.100 | 0.182 | 0.100 | −0.319 | 0.312 | −0.319 | 0.312 | −2.98 | −2.57 | −2.77 | −2.77 |
| Ge | 0.163 | 0.094 | 0.163 | 0.094 | −0.501 | 0.247 | −0.501 | 0.247 | −3.40 | −2.67 | −3.03 | −3.03 |
| Sn | 0.131 | 0.077 | 0.131 | 0.077 | −0.533 | 0.120 | −0.533 | 0.120 | −3.61 | −2.70 | −3.16 | −3.16 |
| Pb | 0.077 | 0.058 | 0.077 | 0.058 | −0.798 | −0.040 | −0.798 | −0.040 | −4.96 | −2.82 | −3.89 | −3.89 |
| NR-Pb | 0.101 | 0.060 | 0.101 | 0.606 | −0.547 | −0.022 | −0.547 | −0.022 | −3.76 | −2.85 | −3.31 | −3.31 |

In Table III we compare the calculated covalent and ionic average gap components, $E_h^*$ and $C^*$, to the spectroscopic values derived by Phillips.[1] Also, we compare the ionicity values $f_i^*$ calculated from Eq. (33) to the Phillips ionicity $f_i$. In the last two rows of Table III we give results for Pb calculated for the (hypothetical) diamond structure. The row labeled NR-Pb contains results where all relativistic corrections are excluded. Relativistic effects are very important for the bonding properties of Pb. The mass-velocity downshift of the 6*s* states with respect to the 6*p* levels is so large that the formation of strong $sp^3$ covalent bonds becomes unfavorable,[28] and the crystal structure which is stable at ambient conditions is the face-centered cubic. Omitting all relativistic effects we found[28] that the diamond structure of Pb has a lower total energy than the fcc. The bonding properties of NR-Pb are quite similar to those of Sn.

The results in Table III show that the ionicities calculated in our model exhibit the same chemical trends as those found in the values derived from the Phillips–van Vechten theory. In general, our ionicities tend to be somewhat larger than $f_i$. At least in one case, SiC, we feel that our larger value gives a more adequate description of the ionicity than Phillips value. This was mentioned in Sec. II. A general comparison of the theoretical ionicities $f_i^*$ to the Phillips scale is given in Fig. 6.

The $sp^3$ bonding and antibonding characters, $\mathcal{B}$ and $\mathcal{A}$, and the bond orders $b = \mathcal{B} - \mathcal{A}$ as derived from Eq. (21) (and the equivalent for $\mathcal{A}$) are given for some of the compounds in Table IV. Apart from a few cross-row compounds (listed at the bottom as InAs,AlAs, InP, and SiC), results are given only for in-row compounds. For these, the results are given first for the first row of the Periodic Table (C, BN, BeO, IV-IV, III-V, II-VI), then for the second, etc. In the same table, Table IV, we again list the bond length $d$ which is the experimental value. This is (third column) compared to the theoretical equilibrium value, $d^{\text{th}}$, obtained by minimizing the total energy (see also Sec. IV, Fig. 11).

Table IV includes columns labeled $d_0$, $d'$ and $\zeta$. The latter is the *internal-strain* parameter as defined by Kleinmann.[29] The quantities $d_0$ and $d'$ are deformation poten-

TABLE III. Bond length, $d$, ionic and covalent gaps $C$ [$=\Delta E_{sp^3}$, Eqs. (29) and (30)] and $E_h$ [$=-2h$, Eq. (31)], and ionicities $f_i$. Quantities with an asterisk (*) are present calculations, those without are from Ref. 1.

| Compound | $d$ (Å) | $C$ (eV) | $E_h$ (eV) | $C^*$ (eV) | $E_h^*$ (eV) | $f_i$ | $f_i^*$ |
|---|---|---|---|---|---|---|---|
| AlAs | 2.43 | 2.67 | 4.38 | 4.50 | 5.89 | 0.274 | 0.367 |
| AlP | 2.36 | 3.14 | 4.72 | 5.16 | 6.04 | 0.307 | 0.421 |
| AlSb | 2.66 | 2.07 | 3.53 | 2.38 | 6.38 | 0.250 | 0.163 |
| BAs | 2.07 | 0.38 | 6.55 | 0.35 | 8.33 | 0.002 | 0.002 |
| BN | 1.52 | 7.71 | 13.1 | 9.35 | 11.87 | 0.256 | 0.383 |
| BP | 1.97 | 0.68 | 7.44 | 0.254 | 8.70 | 0.006 | 0.001 |
| BeO | 1.65 | 13.9 | 11.5 | 18.28 | 9.21 | 0.602 | 0.798 |
| BeS | 2.10 | 3.99 | 6.31 | 7.13 | 6.62 | 0.286 | 0.537 |
| BeSe | 2.20 | 3.36 | 5.65 | 5.84 | 6.86 | 0.261 | 0.420 |
| BeTe | 2.40 | 2.05 | 4.54 | 3.26 | 6.16 | 0.169 | 0.222 |
| CdS | 2.53 | 5.90 | 3.97 | 9.19 | 4.67 | 0.685 | 0.794 |
| CdSe | 2.63 | 5.50 | 3.61 | 8.35 | 3.62 | 0.699 | 0.841 |
| CdTe | 2.81 | 4.90 | 3.08 | 6.35 | 3.77 | 0.717 | 0.739 |
| CuBr | 2.47 | 6.90 | 4.14 | 17.75 | 6.66 | 0.735 | 0.877 |
| GaAs | 2.45 | 2.90 | 4.32 | 4.29 | 6.40 | 0.310 | 0.310 |
| GaP | 2.36 | 3.30 | 4.73 | 5.00 | 6.66 | 0.327 | 0.361 |
| GaSb | 2.65 | 2.10 | 3.55 | 2.08 | 5.95 | 0.261 | 0.108 |
| HgPo | 2.93 | | | 5.71 | 3.58 | | 0.718 |
| HgTe | 2.80 | 4.0 | 5.0 | 5.82 | 3.96 | 0.65 | 0.74 |
| InAs | 2.62 | 2.74 | 3.67 | 5.06 | 4.55 | 0.357 | 0.553 |
| InP | 2.54 | 3.34 | 3.93 | 6.15 | 5.68 | 0.421 | 0.534 |
| InSb | 2.81 | 2.10 | 3.08 | 3.39 | 5.13 | 0.321 | 0.303 |
| MgS | 2.44 | 7.10 | 3.71 | 9.75 | 4.44 | 0.786 | 0.828 |
| SiC | 1.88 | 3.85 | 8.27 | 7.47 | 9.27 | 0.177 | 0.394 |
| SiGe | 2.42 | | | 0.06 | 6.08 | | 0.0001 |
| ZnPo | 2.70 | | | 7.79 | 6.59 | | 0.582 |
| ZnS | 2.34 | 6.20 | 4.82 | 8.57 | 4.76 | 0.623 | 0.764 |
| ZnSe | 2.45 | 5.60 | 4.29 | 12.51 | 7.41 | 0.630 | 0.740 |
| ZnTe | 2.64 | 4.48 | 3.59 | 5.60 | 4.97 | 0.609 | 0.560 |
| C | 1.54 | 0 | 13.5 | 0 | 13.31 | 0.000 | 0.000 |
| Si | 2.35 | 0 | 4.77 | 0 | 6.82 | 0.000 | 0.000 |
| Ge | 2.45 | 0 | 4.31 | 0 | 6.38 | 0.000 | 0.000 |
| Sn | 2.84 | 0 | 3.06 | 0 | 5.18 | 0.000 | 0.000 |
| Pb | 3.17 | | | 0 | 3.75 | 0.000 | 0.000 |
| NR-Pb | 3.17 | | | 0 | 3.95 | 0.000 | 0.000 |

TABLE IV. Experimental ($d$) and theoretical ($d^{\text{th}}$), bond lengths, $sp^3$ bonding characters ($\mathcal{B}$), bond orders ($\mathcal{B}-\mathcal{A}$), optical deformation potentials $d_0,d'$) entering Eq. (47) and internal-strain parameter ($\zeta$). The last column gives the $\zeta$ values [$\zeta$(int)] obtained by "chemical interpolation" (cf. Fig. 7). (*Note added.* Since the submission of this paper we have calculated $d_0$ and $d'$ with the inclusion of the nonspherical parts of the potentials [L. Brey, N. E. Christensen, and M. Cardona, Phys. Rev. B (to be published)]. The corrections to the deformation potentials are large, but the chemical trends as discussed here are not affected, and the $\zeta$ values are almost unchanged.)

| Compound | $d$ (Å) | $d^{\text{th}}$ (Å) | $\mathcal{B}$ | $b=\mathcal{B}-\mathcal{A}$ | $d_0$ (eV) | $d'$ (eV) | $\zeta$ | $\zeta$(int) |
|---|---|---|---|---|---|---|---|---|
| C | 1.54 | 1.54 | 0.770 | 0.760 | 53.8 | −2.35 | | 0.28 |
| BN | 1.57 | 1.57 | 0.675 | 0.706 | 32.7 | −3.80 | | 0.41 |
| BeO | 1.65 | 1.64 | 0.685 | 0.529 | 13.3 | −3.29 | | 0.75 |
| Si | 2.35 | 2.35 | 0.725 | 0.687 | 22.7 | −2.46 | 0.50 | 0.45 |
| AlP | 2.36 | 2.38 | 0.697 | 0.622 | 14.9 | −3.34 | | 0.58 |
| MgS | | 2.44 | 0.662 | 0.508 | 6.83 | −3.07 | | 0.80 |
| Ge | 2.45 | 2.45 | 0.720 | 0.670 | 23.6 | −2.27 | 0.46 | 0.48 |
| GaAs | 2.45 | 2.45 | 0.719 | 0.644 | 17.5 | −2.20 | 0.53 | 0.53 |
| ZnSe | 2.45 | 2.45 | 0.698 | 0.587 | 7.53 | −2.95 | 0.45 | 0.64 |
| CuBr | 2.49 | 2.44 | 0.690 | 0.490 | −4.26 | −1.54 | 0.83 | 0.82 |
| Sn | 2.80 | 2.84 | 0.710 | 0.660 | | | | 0.50 |
| InSb | 2.81 | 2.82 | 0.723 | 0.604 | 14.6 | −2.63 | 0.65 | 0.61 |
| CdTe | 2.81 | 2.83 | 0.692 | 0.581 | 6.33 | −2.78 | 1.28 | 0.65 |
| AlAs | 2.43 | 2.45 | 0.700 | 0.620 | 15.7 | −3.27 | | 0.58 |
| InAs | 2.63 | 2.64 | 0.715 | 0.625 | 14.3 | −2.65 | 0.27 | 0.52 |
| InP | 2.54 | 2.54 | 0.712 | 0.619 | 14.1 | −3.01 | 0.57 | 0.59 |
| SiC | 1.88 | 1.89 | 0.682 | 0.615 | 19.1 | −5.24 | | 0.59 |

tials defined as follows. With the inclusion of spin-orbit coupling, the valence-band top ($\Gamma_{15}^v$) is split into the fourfold-degenerate $\Gamma_8^+$ and the twofold-degenerate $\Gamma_7^+$ state ("split off"). A deformation of the crystal that displaces the two sublattices relative to each other by $\bar{u}_{\text{rel}}$ causes a splitting of the $\Gamma_8^+$ state by $\Delta\epsilon$. The deformation potential $d_0$ is related to this splitting by[30]

$$\Delta\epsilon=\frac{|\mathbf{u}_{\text{rel}}|}{a}d_0 , \tag{43}$$

where $a$ is the lattice constant. A uniaxial, volume conserving trigonal strain may be expressed in terms of a deformation parameter $\delta$ via the transformation matrix $\underline{E}$ with the elements

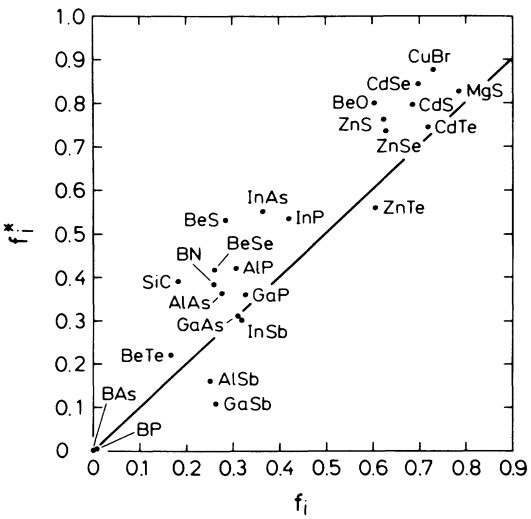


FIG. 6. The ionicities $f_i^*$ as derived from our calculations plotted against $f_i$, Phillips ionicity values.

$$E_{ij}=\begin{cases}\frac{1}{3}(e^{\delta}+2e^{-\delta/2}) & \text{for } i=j ,\\ \frac{1}{3}(e^{\delta}-e^{-\delta/2}) & \text{for } i\neq j .\end{cases} \tag{44}$$

With the cation, for example, located at (0,0,0) and the anion at $\mathbf{R}_a=(1,1,1)a/4$ before the strain, the anion position in the strained crystal (strain axis [111]) is

$$\mathbf{R}_a'=[\underline{E}-\zeta(\underline{E}-\underline{1})]\mathbf{R}_a , \tag{45}$$

where $\zeta$ is the internal-strain parameter mentioned above. The splitting $\delta\omega$, caused by this strain ($\delta\rightarrow 0$) of $\Gamma_8^+$ is

$$\delta\omega=3^{1/2}d\delta , \tag{46}$$

where the deformation potential $d$ is

$$d=d'-\tfrac{1}{4}d_0\zeta . \tag{47}$$

The values of $d'$ and $d_0$ given in Table IV were obtained by calculating $d$ by means of the LMTO method for strained crystals with two choices of $\zeta$, and then using the relation (47). The internal-strain parameters listed in Table IV were then derived from Eq. (47) with the experimental value of $d$. The measured deformation potentials were taken from Table 4 of Ref. 31 and from Ref. 32. The magnitude of the internal-strain parameter and its comparison to experiments is discussed for particular cases, elsewhere.[33,34] Here we wish to show the chemical trends in $\zeta$ and $d_0$. Intuitively, we would expect the bond order $b=\mathcal{B}-\mathcal{A}$ to be a measure of the covalent bond strength, and therefore that a large value of $b$ should correspond to a small internal strain and vice versa. Figure 7 shows indeed that $\zeta$ decreases with increasing $sp^3$ bond order. For a given trigonal strain, i.e., a certain value of $\delta$ in Eq. (44), we expect that large value of $\mathcal{B}-\mathcal{A}$ would

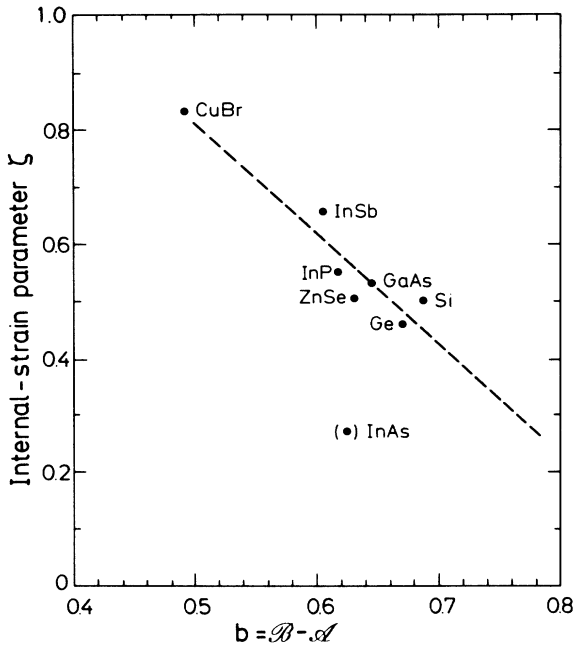


FIG. 7. Internal-strain parameter $\zeta$ versus bond order $b = \mathcal{B} - \mathcal{A}$.

imply that the band splitting would be large; i.e., it is natural to assume, that $d_0$ should increase with increasing bond order. This is also what follows from Fig. 8. The chemical trends in the $d_0$ values are quite similar to those found for $b = \mathcal{B} - \mathcal{A}$.

The valence-force-field theory developed by Keating[35] and further extended by Martin[36] has been useful in the description of the elastic properties of zinc-blende type crystals. In this model, the elastic shear constants $C_{11}$, $C_{12}$, and $C_{44}$ are described in terms of two force constants, $\alpha$ and $\beta$. These are the *bond stretching* ($\alpha$) and *bond bending* ($\beta$) parameters. For a crystal where the covalency is weak, i.e., where the bonding is predominantly ionic, a small value of the ratio $\beta/\alpha$ is expected, whereas a crystal with a large $sp^3$ bond-order value must have a relatively large bond-bending coefficient. This explains the trend of $\beta/\alpha$ (we use the values from Ref. 36) versus $\mathcal{B}/(\mathcal{B}+\mathcal{A})$ as shown in Fig. 9. The trend in Fig. 9 is quite similar to that found in Fig. 3.2.c in Ref. 1, and this comparison also demonstrates that the $sp^3$ bonding part of the total number of $s$ and $p$ $A$ and $B$ electrons decreases with increasing ionicity, as is natural.

The value of $\zeta$ for InAs appears, cf. Fig. 8, to be far too low. A similar anomaly, for this compound, is not found in the $\alpha/\beta$ plot of Fig. 9, and consequently we suggest that the experimental determination of the deformation potential $d = -3.6$ eV (Ref. 32) should be revised.

Table V contains the metallicities $\alpha_m$ and polarities $\alpha_p$ as calculated from Eqs. (39) and (30) from the potential parameters. For comparison we also list the values obtained from Harrison's model, Ref. 2. In general we find values of $\alpha_m$ which are somewhat larger than those given by Harrison. This is mainly reflecting the fact that the conduction states are lying too low in energy when calculated—as we do here—within the local-density approximation (LDA). In two cases, GaSb and InP (see the numbers in Table V labeled "$c$" also) we have used self-consistent band structures where the gaps have been adjusted. This was done by adding very sharply peaked external potentials on the atomic sites.[37] With these adjustments we see (Table V) that $\alpha_m$ is reduced and, in fact, very close to the values of Ref. 2. As mentioned earlier, the down-folding procedure is very important to the

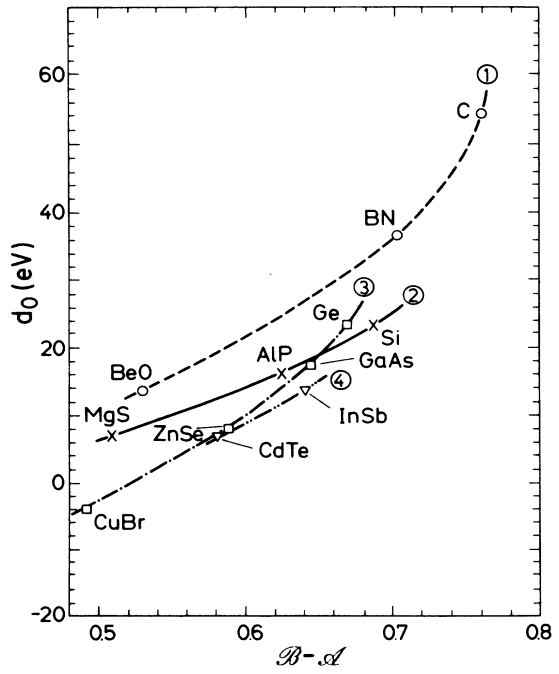


FIG. 8. Deformation potential $d_0$ versus $sp^3$-bond order $b = \mathcal{B} - \mathcal{A}$. (See also *Note added* in the caption to Table IV.)

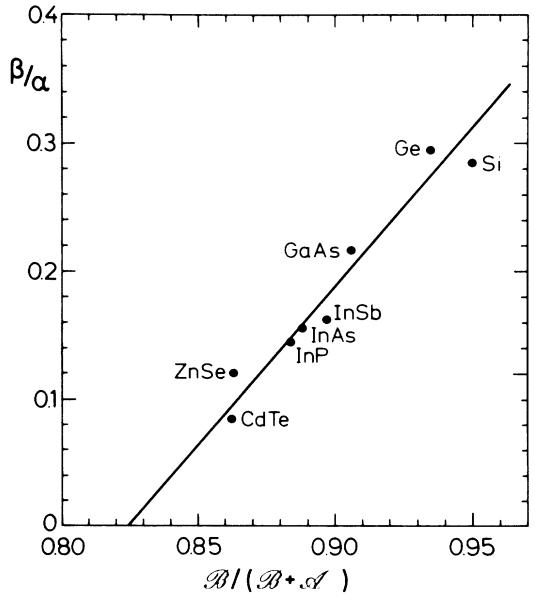


FIG. 9. Ratio $\beta/\alpha$ of bond-bending and bond-stretching force constants versus the calculated values of $\mathcal{B}/(\mathcal{B}+\mathcal{A})$.

TABLE V. Polarities ($\alpha_p$) and metallicities ($\alpha_m$) as derived from Eqs. (36)–(40). Our results are compared to those obtained by Harrison (Ref. 2).

| Compound | Polarity $\alpha_p$ | | Metallicity $\alpha_m$ | |
|---|---|---|---|---|
| | Ref. 2[a] | This work | Ref. 2[b] | This work |
| AlAs | 0.44 | 0.38 | 0.64 | 0.76 |
| AlP | 0.47 | 0.47 | 0.57 | 0.67 |
| AlSb | 0.54 | 0.19 | 0.68 | 0.85 |
| BAs | 0.00 | −0.19 | 0.55 | 0.66 |
| BN | 0.41 | 0.45 | 0.34 | 0.36 |
| BP | 0.00 | −0.08 | 0.47 | 0.57 |
| BeO | 0.64 | 0.78 | 0.37 | 0.29 |
| BeS | 0.21 | 0.50 | 0.42 | 0.52 |
| BeSe | 0.32 | 0.33 | 0.47 | 0.57 |
| BeTe | 0.00 | 0.13 | 0.48 | 0.66 |
| CuBr | 0.79 | 0.91 | 0.44 | 0.63 |
| CdS | 0.77 | 0.77 | 0.48 | 0.60 |
| CdSe | 0.77 | 0.82 | 0.54 | 0.73 |
| CdTe | 0.76 | 0.75 | 0.49 | 0.84 |
| GaAs | 0.50 | 0.40 | 0.71 | 0.83 |
| GaP | 0.52 | 0.49 | 0.62 | 0.74 |
| GaSb | 0.44 | 0.20, 0.20[c] | 0.74 | 0.90, 0.78[c] |
| HgPo | | 0.65 | | 1.08 |
| HgTe | | 0.691 | | 0.949 |
| InAs | 0.53 | 0.59 | 0.71 | 0.95 |
| InP | 0.58 | 0.61, 0.61[c] | 0.63 | 0.73, 0.66[c] |
| InSb | 0.51 | 0.40 | 0.74 | 0.91 |
| MgS | | 0.79 | | 0.51 |
| SiC | 0.39 | 0.54 | 0.45 | 0.50 |
| SiGe | | −0.07 | | 0.94 |
| ZnPo | | 0.64 | | 0.98 |
| ZnS | 0.73 | 0.77 | 0.47 | 0.68 |
| ZnSe | 0.72 | 0.81 | 0.53 | 0.76 |
| ZnTe | 0.72 | 0.59 | 0.53 | 0.83 |
| C | 0 | 0 | 0.34 | 0.37 |
| Si | 0 | 0 | 0.66 | 0.76 |
| Ge | 0 | 0 | 0.81 | 0.99 |
| Sn | 0 | 0 | 0.87 | 1.06 |
| Pb | | 0 | | 1.95 |
| NR-Pb | | 0 | | 1.14 |

[a]Table 6-2.
[b]Table 4-1.
[c]Adjusted.

tight-binding value obtained for the $E_0$ gap, and thus to the metallicity. The results quoted so far therefore were obtained with this down folding. Without it we would get $\alpha_m$ values which are considerably larger. For example, the Si value would be $\alpha_m = 0.97$ instead of 0.76, and for Sn the scheme without down folding gives $\alpha_m = 1.34$ as opposed to 1.06 (Table V). The close agreement between the metallicities and polarities as derived from our scheme and those given by Harrison[2] (Table V) clearly shows that it is possible to establish, in a simple manner, a relation between the first-principles electronic structure theories and the parameters entering the more empirically based models. In this way we can, from the first-principles calculations, derive the quantities which traditionally are used to describe the physical and chemical trends in the tetrahedrally bonded compounds. In addition we can, from self-consistent calculations carried out at different volumes, calculate the volume and pressure dependences of these parameters.

We have already (Table II) specified the volume variation of the interatomic matrix elements. In Table VI the volume derivative $df_i^*/d\ln V$, $d\alpha_m/d\ln V$, and $d\alpha_p/d\ln V$ are listed. With a few exceptions (e.g., SiC) we find that $df_i^*/d\ln V$ is positive, i.e., most compounds become *less* ionic when compressed. This result may seem surprising in view of the remarks in the Introduction claiming that a larger ionicity value tends to stabilize the crystal structure with the high (6) coordination number *and* that the zinc-blende-type crystals under pressure transform to the rocksalt structure. The ionicity itself, however, is not directly a measure of the ionic interaction *energy*. This scales, for fixed charges, in its simplest approximation, with the inverse of the lattice constant. The ionicity, on the other hand, is rather a measure of the di-

TABLE VI. Volume coefficients $d(x)/d\ln V$ of $x = E_h^*$ $C^*$, $f_i^*$, $\alpha_p$, and $\alpha_m$.

| Compound | $\frac{dE_h^*}{d\ln V}$ (eV) | $\frac{dC^*}{d\ln V}$ (eV) | $\frac{df_i^*}{d\ln V}$ | $\frac{d\alpha_p}{d\ln V}$ | $\frac{d\alpha_m}{d\ln V}$ |
|---|---|---|---|---|---|
| AlAs | −4.57 | −1.19 | 0.369 | 0.213 | 0.478 |
| AlP | −5.10 | −2.28 | 0.235 | 0.143 | 0.416 |
| AlSb | −4.69 | 1.09 | 0.379 | 0.358 | 0.547 |
| BAs | −6.57 | −4.89 | −0.043 | 0.336 | 0.525 |
| BN | −10.48 | −5.42 | 0.200 | 0.110 | 0.359 |
| BP | −7.41 | −0.63 | −0.002 | 0.310 | 0.444 |
| BeO | −8.81 | −10.09 | 0.185 | 0.101 | 0.195 |
| BeS | −5.88 | −0.50 | 0.487 | 0.387 | 0.269 |
| BeSe | −5.81 | 1.07 | 0.591 | 0.459 | 0.260 |
| BeTe | −5.10 | 3.99 | 0.743 | 0.687 | 0.341 |
| CdS | −6.67 | −6.64 | 0.477 | 0.434 | 0.536 |
| CdSe | −5.40 | −6.67 | 0.197 | 0.139 | 0.360 |
| CdTe | −5.35 | −2.87 | 0.407 | 0.306 | 0.425 |
| CuBr | −5.08 | −7.14 | 0.092 | 0.047 | 0.085 |
| GaAs | −5.97 | −1.44 | 0.342 | 0.238 | 0.700 |
| GaP | −5.55 | −2.34 | 0.266 | 0.175 | 0.649 |
| GaSb | −5.96 | 1.62 | 0.363 | 0.426 | 0.928 |
| HgPo | −3.96 | −0.84 | 0.450 | 0.335 | 0.305 |
| HgTe | −4.31 | −2.00 | 0.336 | 0.206 | 0.418 |
| InAs | −4.00 | −3.16 | 0.171 | 0.077 | 0.681 |
| InP | −5.07 | −4.43 | 0.221 | 0.138 | 0.679 |
| InSb | −5.65 | −0.71 | 0.478 | 0.389 | 0.957 |
| MgS | −4.24 | −5.34 | 0.161 | 0.106 | 0.218 |
| SiC | −5.81 | −7.04 | −0.114 | −0.103 | 0.436 |
| SiGe | −5.35 | −0.68 | −0.002 | 0.047 | 0.830 |
| ZnPo | −5.27 | 0.31 | 0.488 | 0.386 | 0.305 |
| ZnS | −4.88 | −4.47 | 0.190 | 0.087 | 0.299 |
| ZnSe | −5.58 | −5.91 | 0.127 | 0.052 | 0.184 |
| ZnTe | −5.39 | −0.26 | 0.553 | 0.391 | 0.403 |
| C | −9.21 | 0 | 0 | 0 | 0.391 |
| Si | −5.21 | 0 | 0 | 0 | 0.566 |
| Ge | −5.07 | 0 | 0 | 0 | 0.928 |
| Sn | −4.15 | 0 | 0 | 0 | 1.142 |
| Pb | −3.32 | 0 | 0 | 0 | 2.720 |

pole moment, i.e., ionic charge *times* bond length. In terms of ionicity values the pressure-induced $N_C=4\rightarrow N_C=6$ transition should rather be considered as a result of a competition between the decrease of $f_i$ with pressure and a more rapid *decrease* of the *critical* ionicity separating the two types of crystal structure. (We shall comment further on this decrease after the discussion of the total-energy calculations, Sec. IV.) The few compounds (like SiC) where $df_i^*/dP$ is positive would then be expected to have an "unusually" strong tendency to transform to the rocksalt structure. The total-energy calculations in the next chapter support this.

A connection between ionicities or polarities and effective ionic charges is not easily established. The defintion of the charge depends critically on what physical quantity is assumed to be measured. It is customary to define a "transverse effective charge," $e_T^*$ from the longitudinal- and transverse-optical-phonon frequencies:

$$\omega_{\mathrm{LO}}^2-\omega_{\mathrm{TO}}^2=\frac{2\pi^2(e_T^*)^2}{M\Omega_0\epsilon}\ , \tag{48}$$

where $\epsilon$ is the dielectric constant, $\Omega_0$ the cell volume, and $M$ is the reduced mass.

Using a derivation analogous to that given in Chap. 9 of Ref. 2 we find

$$e_T^*=4\left[\alpha_p+\frac{d\alpha_p}{d\ln V}\right]-\Delta Z\ , \tag{49}$$

where $\Delta Z$ is the anion-cation atomic number difference. [The relation (9-24) in Ref. 2 assumes the $d^{-2}$ scaling of the interatomic matrix elements. We use $d\alpha_p/d\ln V$ as calculated directly here (Table VI)]. Another effective charge, the piezoelectric charge, $e_P^*$, is defined in terms of the strain-induced polarization density

$$P_x=\frac{\zeta a e e_P^*}{8\Omega_0}\epsilon_{yz}\ , \tag{50}$$

where $\zeta$ is the internal-strain parameter discussed previously. Using again a derivation similar to that of Har-

rison,[2] we get

$$e_P^* = 4\left[\alpha_p - \frac{1-\zeta}{\zeta}\frac{d\alpha_p}{d\ln V}\right] - \Delta Z \ . \quad (51)$$

The derivations of (49) and (51) are approximate as pointed out in Ref. 2. Further, it is not obvious whether one should use $\alpha_p$ as defined in (40) which refers to $p$ states only or a polarity defined in terms of the hybrids. In the latter case we would replace $\alpha_p$ by $(f_i^*)^{1/2}$.

The effective charges $e_T^*$ and $e_P^*$ are tabulated in Table VII, where we again compare our data to Harrison's calculations and to experiments where such data are available. The piezoelectric charge, Eq. (51), depends sensitively on the internal-strain parameter. We use here the values which we have calculated (Table IV). As in the case of the calculations in Ref. 2, the agreement between the theoretical and experimental values of $e_T^*$ and $e_P^*$ is only semiquantitative. As follows from the column labeled $\epsilon_T^*$(hyb) in Table VII, the agreement, in the case of $e_T^*$, is improved if we use the hybrid values $(f_i^*)^{1/2}$, instead of $\alpha_p$, as suggested above.

It should be stressed that Eqs. (49) and (51) are derived with the assumption that the bond-length dependences can be obtained simply from the volume dependences. This approximation may be particularly bad in our TB scheme which contains volume-dependent diagonal matrix elements. The bond-length scalings of the off-diagonal elements in a volume-conserving distortion may thus differ from the one which we have used.

## IV. TOTAL-ENERGY CALCULATIONS

In this section we give the results of the calculated volume dependences of the total energies and the structural energy differences. In particular we shall discuss the relative stability of the rocksalt ($B1$) and the zinc-blende ($B3$) structures. From these calculations it will be shown that a critical ionicity value separates the fourfold- and sixfold-coordinated structures. The total energies are calculated within the local-density approximation, and we use the Barth-Hedin scheme.[9]

First we show, in Fig. 10, an example of theoretical pressure-volume relations. We have chosen to show the results for diamond, since a detailed comparison to another, recent calculation[38] is possible in that case. The LMTO and pseudopotential[38] calculations agree extremely well. The fact that our pressure calculation (see the table inset in Fig. 10) appears to agree slightly better with experiments than Nielsen's data is probably fortuitous. In Fig. 11 we compare the theoretical equilibrium bond lengths to the experimental values. The straight line indicates exact agreement. The root-mean-square error in the theoretical values is less than 0.2%. The largest errors are found for ZnTe and CuBr. A more detailed comparison between the theoretical and experimental equilibrium lattice constant is given in Table IV for some of the compounds.

According to the structural phase diagram calculated by Chelikowsky and Burdett[10] we would expect that the IV-IV compound SiC under pressure should undergo a transition from the zinc-blende structure to the $\beta$-Sn structure. In order to examine this, within the framework of our total-energy calculations, we compare in Fig. 12 the volume variation of the total energy of SiC in these three structures. For the $\beta$-Sn structure we have assumed that the $c/a$ ratio is $\sqrt{4/15}=0.5164$. In that case the coordination number is 6, i.e., the same as that of the rocksalt structure. According to our calculations, Fig. 12, the cubic SiC is expected to go to the $B1$ structure under compression, and *not* to the $\beta$-Sn structure. The calculated pressure of the $B3 \rightarrow B1$ transition is $P_t \simeq 590$ kbar. This is obtained from the calculated enthalpy as a function of pressure. This result is thus in contrast to that of Ref. 10, but it does, of course, not invalidate the general

TABLE VII. Effective charges $e_T^*$ and $e_P^*$ derived from Eqs. (49) and (51). The quantity $e_T^*$ (hyb) was obtained from Eq. (49) with $\alpha_p$ replaced by $(f_i^*)^{1/2}$. The $e_P^*$ values labeled ($a$) were calculated with $\zeta=\zeta$(int) (Table IV).

| Compound | $e_T^*$ Ref. 2 | $e_T^*$ This calculation | $e_T^*$(hyb) This calculation | $e_T^*$ Expt. | $e_P^*$ Ref. 2 | $e_P^*$ This calculation | $e_P^*$ Expt. |
|---|---|---|---|---|---|---|---|
| AlAs | 1.91 | 1.38 | 2.49 | 2.3 | 0.46 | −0.08(a) | |
| AlP | 2.03 | 1.46 | 2.32 | 2.28 | 0.59 | 0.46(a) | |
| AlSb | 1.78 | 1.19 | 2.49 | 1.93 | 0.46 | | −0.22 |
| BAs | −0.26 | −0.41 | −2.72 | | −0.68 | | |
| BN | 1.17 | 1.23 | 2.11 | 2.47 | 0.11 | 0.15(a) | |
| BP | −0.38 | −0.08 | −1.06 | | −0.61 | | |
| BeO | 1.12 | 1.51 | 1.98 | 1.83 | −0.15 | 0.97(a) | −0.13 |
| BeS | −1.32 | 1.53 | 2.26 | | −0.34 | | |
| BeSe | 1.49 | 1.17 | 2.42 | | −0.13 | | |
| BeTe | −1.19 | 1.29 | 3.04 | | −0.37 | | |
| CuBr | 1.04 | 0.82 | 0.94 | 1.49 | 0.42 | 0.59 | |
| CdS | 1.97 | 2.80 | 2.64 | 2.77 | 1.12 | | 0.06 |
| CdSe | 1.95 | 1.86 | 2.10 | 2.25 | 1.08 | | 0.52 |
| CdTe | 1.94 | 2.21 | 2.39 | 2.35 | 1.01 | 1.25 | 0.09 |
| GaAs | 1.92 | 1.56 | 2.26 | 2.16 | 0.47 | −0.23 | −0.47 |
| GaP | 2.43 | 1.65 | 2.29 | 2.04 | 0.90 | | −0.28 |
| GaSb | 1.74 | 1.53 | 2.52 | 2.15 | 0.36 | | −0.42 |
| HgTe | | 2.12 | 1.59 | | | | |

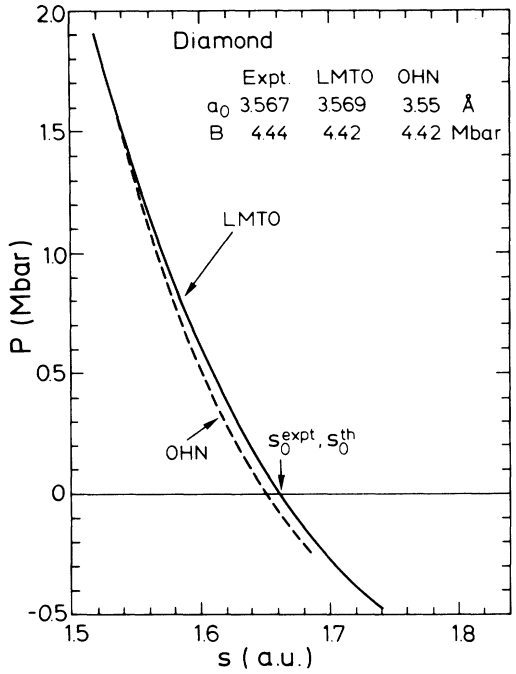


FIG. 10. Pressure $P$ vs atomic-sphere radius $s$ for diamond. The lattice constant $a = s(64\pi/3)^{1/3}$. The curve labeled OHN represents the pseudopotential calculation by Nielsen (Ref. 38). The curve drawn with a solid line is the present LMTO result. The theoretical equilibrium lattice constants ($a_0$) and bulk moduli ($B$) are compared to experimental values in the table inserted.

qualitative trends found in that work[10] that a specific compound behaves differently. We have already mentioned, in Secs. II and III, that SiC according to our calculations is more ionic than is often assumed. Further, we found that $df_i^*/dP$ ($P$ being the pressure) is positive

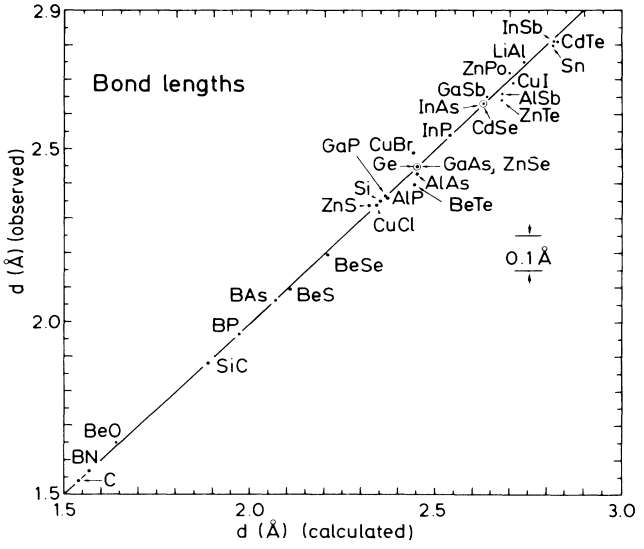


FIG. 11. The observed equilibrium bond lengths vs the theoretical values obtained by minimizing the total energy. All calculations are made for the zinc-blende (diamond) structure. (See also Table IV.)

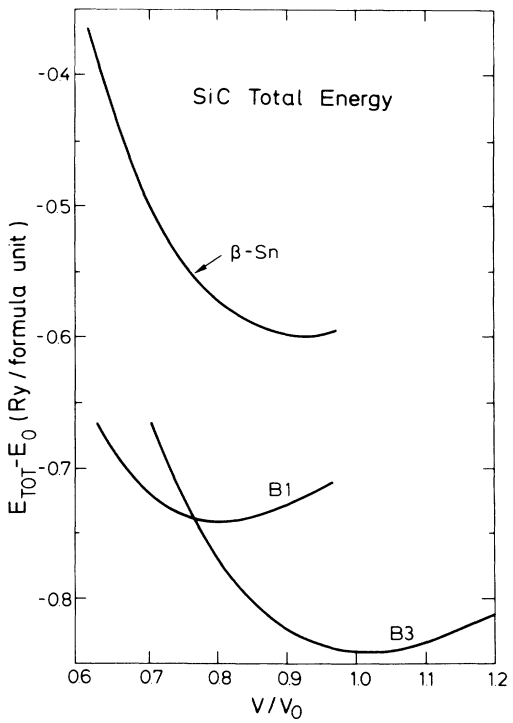


FIG. 12. Calculated total energies of SiC vs volume ratio, $V/V_0$ ($V_0$ is the equilibrium volume in the $B3$ structure), in three crystal structures, zinc blende ($B3$), rocksalt ($B1$), and $\beta$-Sn. The $c/a$ ratio for the $\beta$-Sn structure was taken to be the ideal, $c/a = \sqrt{4/15}$. With this choice, the coordination number is $N_C = 6$, i.e., the same as in $B1$.

in that case.

By means of the "frozen-potential method" (FPM) for calculations of structural energy differences at fixed volumes,[8] we have elsewhere[7] demonstrated for CdTe and ZnTe that the ionic electrostatic interaction drives the pressure-induced $B3$-$B1$ transition. Within the FPM, the structural energy difference[39] is given by

$$\Delta E = \Delta \sum_i^{\text{occ}} \varepsilon_i + \Delta E^{\text{STR}}_{\text{Madelung}} + \Delta E(\Delta\rho) \ , \tag{52}$$

where the first term is the difference in the one-electron energy sum, $\Delta E^{\text{STR}}_{\text{Madelung}}$ is the structural difference in Madelung energy, with fixed charges,[39] and the last term is the (complicated) charge-redistribution contribution. This latter term, however, in our case is small[39] compared to the first two, and the relative stability of the $B3$ and $B1$ structures may thus be viewed as a competition between the "band-structure term," $\Delta \sum_i \varepsilon_i$, and the ionic term, $\Delta E^{\text{STR}}_{\text{Madelung}}$. The former contains the contributions from hybridization and covalent bond formation, and it will therefore tend to stabilize the covalently bonded structure $B3$. The second term, on the other hand, favors the structure with the larger coordination number, i.e., $B1$.

Two examples of calculations using the FPM are shown in Figs. 13 and 14. In both cases the compounds are of type III-V, but their ionicities are quite different. The more ionic compound, AlP (Fig. 13) is much more easily transformed into the rocksalt structure than the

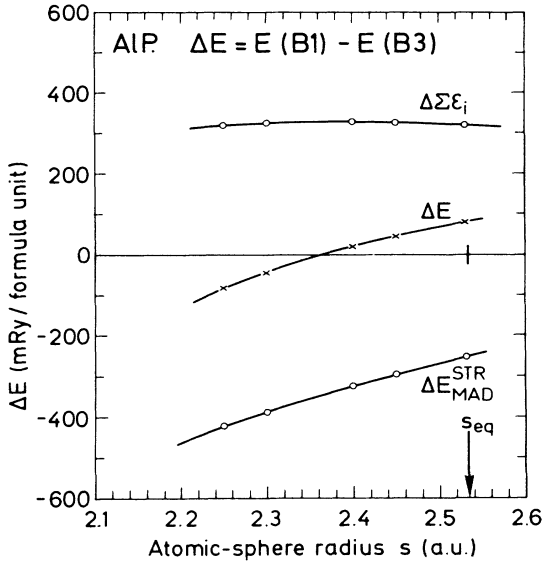


FIG. 13. Structural energy difference, $\Delta E = E(B1) - E(B3)$, calculated for AlP by means of the frozen-potential method [Eq. (52)]. The two most important contributions, $\Delta \sum_i \varepsilon_i$ and $\Delta E^{\mathrm{STR}}_{\mathrm{Madelung}}$ are also shown. The abscissa value indicated by $s_{\mathrm{eq}}$ gives the atomic-sphere radius corresponding to the equilibrium volume of the zinc-blende structure ($B3$).

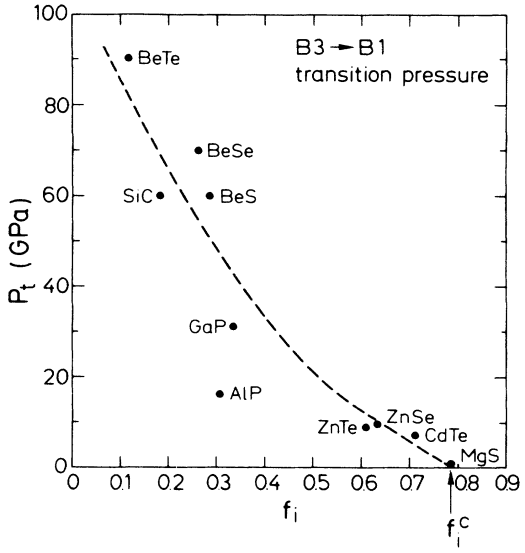


FIG. 15. Calculated pressure $P_t$ for the transition from the sphalerite ($B3$) to the rocksalt structure ($B1$) vs the spectroscopic (Phillips) ionicity.

compound BAs (Fig. 14), which at $P=0$ has the ionicity value close to 0.

We may try to relate the pressure-induced $B3$-$B1$ transitions to the "compositional" structure change, i.e., the $B3 \rightarrow B1$ transition observed in the Phillips–van Vechten theory at the critical ionicity $f_i^c = 0.786$. We do this by calculating, for each compound, the pressure $P_t$ of the $B3 \rightarrow B1$ transition and to study the trends in $P_t(f_i^*)$ or $P_t(f_i)$. In Fig. 15 we have plotted the theoretical transition pressures for ten compounds versus Phillips ionicity.

It follows that $P_t$ goes to zero for $f_i \simeq 0.8$, i.e, in agreement with the critical ionicity value $f_i = 0.786$ found from the zero-pressure analysis in terms of the Phillips–van Vechten theory. Also our ionicity values $f_i^*$ exhibit a similar limiting behavior when related to $P_t$. This follows from Fig. 16. In this case, however, the results seem to separate two groups of data as tentatively indicated by the two straight lines, both, however, with the same $P_t = 0$ limit ($\sim 0.8$). Among the compounds included here, the group in Fig. 16 with the higher $P_t$ values appear to be these where one of the constituent atoms (Be or C) have no $p$ states in the core. Those with $p$-like core states in both atoms (GaP, AlP, ZnTe, ZnSe, CdTe) all lie very

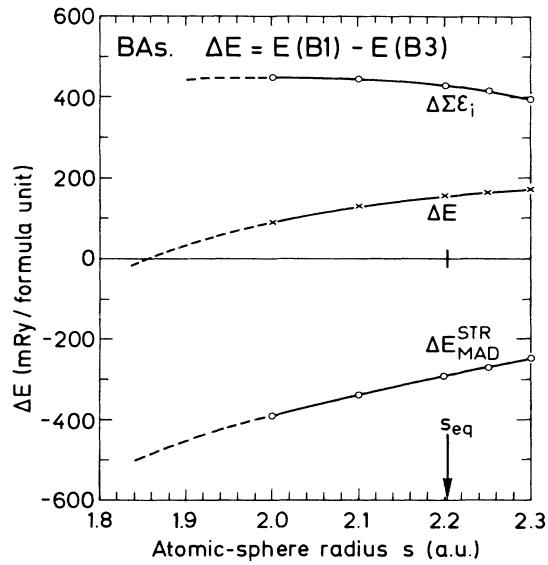


FIG. 14. As Fig. 13, but for BAs. The dashed parts of the curves are guessed extrapolations.

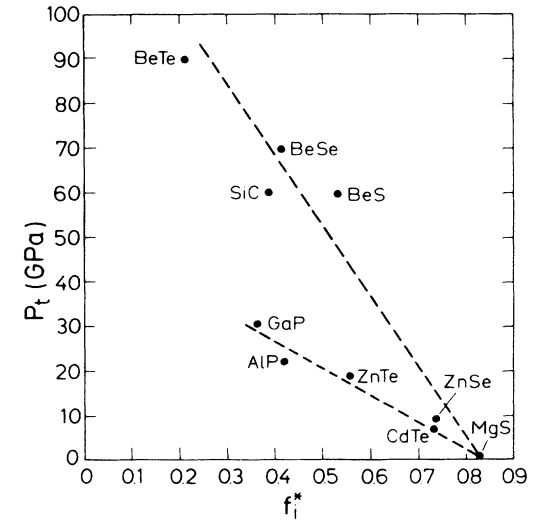


FIG. 16. Theoretical transition pressure versus theoretical ionicity $f_i^*$.

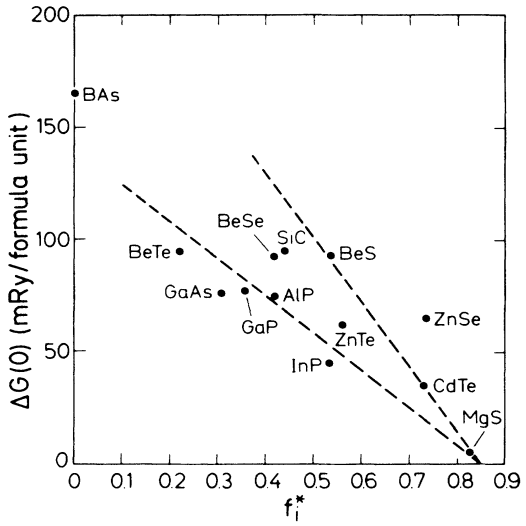


FIG. 17. Structural difference $\Delta G(0)$ between the minimum (i.e., $P=0$ values) of the total energies in the $B1$ and $B3$ structures vs $f_i^*$.

close to the lower line in Fig. 16.

Finally we show, in Fig. 17, dependence on ionicity of the structural difference in free energy at zero pressure, $\Delta G(0)$. [This is not the same as obtained directly from Eq. (52) which is the difference at a given *volume*.] This again suggests the existence of an upper value of $f_i^*$ above which $\Delta G(0)$ would be negative.

In the preceding section we demonstrated that the ionicity in almost all compounds decrease with pressure, and explained the pressure-induced $B3 \rightarrow B1$ transition in terms of the more rapidly decreasing *critical* ionicity. This picture is clear in view of the calculations presented in this chapter. The negative slope of the dashed line in Fig. 15 alone is evidence for a reduction of the critical ionicity when the lattices are compressed, but the frozen-potential-method calculations show this fact more clearly. The Madelung term derives the $B3 \rightarrow B1$ transition, and even if we neglect changes in the charge distribution upon compression, then this term increases in magnitude simply due to the reduction of the interatomic distances. The ionicity of the compound would in such a case decrease since it in a sense represents a dipole moment. Thus, for the compressed lattice an ionicity smaller than at equilibrium volume may correspond to a $\Delta E^{\mathrm{STR}}_{\mathrm{Madelung}}$ [Eq. (52)] that is large enough in magnitude to drive the structure into $B1$, i.e., the critical ionicity is smaller for compressed crystals.

## V. SUMMARY AND CONCLUSION

First-principles electronic structure calculations and total-energy calculations have been performed for a large number of $A^N B^{8-N}$ binary compounds. The band-structure scheme (LMTO) which was used applied basis sets designed for the purpose of calculation of the specific properties. The bond orders ($sp^3$ bonding and antibonding parts) were evaluated by using the orthogonal basis, whereas the charge densities were calculated in a scheme using the most localized basis functions. The charge-density calculations agree in the bonding regions very well with the most recent pseudopotential calculations. The present method of calculation has no region in space where it is not valid, i.e., the core regions are also treated correctly.

A major aim of the work is to demonstrate how the first-principles calculations can be related to more simple and semiempirical models. The exact transformation to a tight-binding (TB) scheme is well known. We have here transformed to a crude TB scheme with an $8\times 8$ Hamiltonian. In this way the parameters entering Harrison's scheme[2] were derived from the first-principles calculations, and in that way we were able to study the theoretically predicted chemical trends in the bonding characteristics entering the phenomenological models. For example, we have found that the $sp^3$ bond order gives a good description of the degree of covalency of the bond. It gives a quantitative classification of the bond strength which is only semiquantitatively obtained from the charge distribution calculations. As examples of the usefulness of the bond-order parameter ($b$) we have presented the relations between $b$ and the elastic properties (deformation potentials and internal-strain parameters).

It might be argued that several parameters, metallicity ($\alpha_m$), polarity ($\alpha_p$), or ionicity ($f_i$), for example, have been introduced previously, and that it therefore is unnecessary to introduce yet another parameter, the bond order. We do feel, however, that it is a natural physical quantity to calculate when the strength of the $sp^3$ bond is discussed. As opposed to $\alpha_p$ or $f_i$, it has the advantage of specifying the $sp^3$ character directly, and it also distinguishes between the bonding in different homopolar semiconductors.

The connection to the Phillips–van Vechten theory is also established. The ionicities have been calculated using the same definition in terms of the average gap parameters, $E_h$ and $C$, as used in the spectroscopic theory. The agreement between the present theoretical values and the empirical ionicity values is in general very good. There are, however, cases where rather large differences are found. In the case of SiC we find the ionicity to be substantially larger. Apparently this larger value is consistent with experiments, and we explain it as being due to the lack of $p$ states in the C core.

The calculated criteria for structural stability clearly show that the ionicity of the bond is essential in separating the fourfold-coordinated structures from those with $N_c=6$. In agreement with the analysis in Ref. 1 based on the spectroscopic model, our calculations show that a critical ionicity value ($f_i \simeq 0.8$) exists, above which the covalent bonding is not sufficiently strong to stabilize the tetrahedrally bonded crystal structure. The identification of the ionic interaction as the "driving mechanism" in the pressure-induced $B3 \rightarrow B1$ transition has been illustrated by means of the frozen-potential calculations. The ionic interaction *energy* increases in magnitude when the lattice is compressed, but for most compounds (SiC is an exception) *decreases* the ionicity. Roughly speaking, this implies that the critical ionicity decreases with pressure. The analysis established the similarity between the pressure-induced and the compositional $B3 \rightarrow B1$ transition.

*Permanent address: Institute for Low Temperature and Structure Research, Polish Academy of Sciences, P. O. Box 937, PL-50-950 Wrocław, Poland.

[1]J. C. Phillips, *Bonds and Bands in Semiconductors* (Academic, New York, 1973).

[2]W. A. Harrison, *Electronic Structure and the Properties of Solids* (Freeman, San Francisco, 1980).

[3]J. R. Chelikowsky and M. L. Cohen, Phys. Rev. B **14**, 556 (1976).

[4]C. S. Wang and B. M. Klein, Phys. Rev. B **24**, 3393 (1981).

[5]O. K. Andersen, Z. Pawlowska, and O. Jepsen, Phys. Rev. B **34**, 5253 (1986).

[6]Z. Pawlowska, N. E. Christensen, S. Satpathy, and O. Jepsen Phys. Rev. B **34**, 5977 (1986).

[7]N. E. Christensen and O. B. Christensen, Phys. Rev. B **33**, 4739 (1986).

[8]O. K. Andersen and N. E. Christensen (unpublished) [see also N. E. Christensen, Phys. Rev. B **32**, 207 (1985)]. The "frozen-potential" approach is reminiscent of Andersen's "force theorem" [A. R. Mackintosh and O. K. Andersen, in *Electrons at the Fermi Surface,* edited by M. Springford (Cambridge University Press, Cambridge, England, 1979].

[9]The total-energy calculations are carried out within the local approximation (LDA) to the density-functional theory. We apply the LDA parametrization of U. von Barth and L. Hedin, J. Phys. C **5**, 1629 (1972).

[10]J. R. Chelikowsky and J. K. Burdett, Phys. Rev. Lett. **56**, 961 (1986).

[11]We have no way in which we can derive physically meaningful values of "charge transfers." There is no systematic way in which we can divide space in an $AB$ compound into $A$ and $B$ regimes, respectively. Thus we cannot from our *charge-density calculations* directly obtain mapping on the Phillips scale.

[12]G. B. Bachelet and N. E. Christensen, Phys. Rev. B **31**, 879 (1985); N. E. Christensen and G. B. Bachelet, *Proceedings of the International Conference on the Physics of Semiconductors, San Francisco, 1984,* edited by J. D. Chadi and W. A. Harrison (Springer, Berlin, 1985), p. 1009.

[13]**10** A. Goldmann, J. Tejeda, N. J. Shevckik, and M. Cardona, Phys. Rev. B , 4388 (1974); A. Blacha, M. Cardona, N. E. Christensen, S. Ves, and H. Overhof, Solid State Commun. **43**, 183 (1982); A. Blacha, N. E. Christensen, and M. Cardona, Phys. Rev. B **33**, 2413 (1986).

[14]D. R. Hamann, M. Schlüter, and C. Chiang, Phys. Rev. Lett. **43**, 1494 (1979); G. B. Bachelet, D. R. Hamann, and M. Schlüter, Phys. Rev. B **26**, 4199 (1982).

[15]This calculation for GaAs was performed by G. B. Bachelet and E. Molinari.

[16]N. Churcher, K. Kunc, and V. Heine, Solid State Commun. **56**, 177 (1985).

[17]J. R. Chelikowsky and J. C. Phillips, Phys. Rev. B **17**, 556 (1976).

[18]O. K. Andersen, Phys. Rev. B **12**, 3060 (1975).

[19]O. K. Andersen and O. Jepsen, Phys. Rev. Lett. **53**, 2571 (1984).

[20]O. K. Andersen, O. Jepsen, and D. Glötzel, in *Highlights of Condensed Matter Theory* (Soc. Italiana di Fisica, Bologna, Italy, 1985), Corso LXXXIX, p. 59.

[21]W. R. L. Lambrecht and O. K. Andersen, Phys. Rev. B **34**, 2439 (1986).

[22]H. L. Skriver, *The LMTO Method* (Springer, Berlin, 1984).

[23]P. Vogl, H. P. Hjalmarson, and J. D. Dow, J. Phys. Chem. Solids **44**, 365 (1983).

[24]The down folding described in Ref. 21 was applied to the nearly orthogonal representation ($\alpha=\gamma$). The method is equivalent to Löwdin's block perturbation theory, P. O. Löwdin, J. Chem. Phys. **19**, 1396 (1951).

[25]D. Glötzel, B. Segall, and O. K. Andersen, Solid State Commun. **36**, 403 (1980).

[26]S. Satpathy and Z. Pawlowska (unpublished).

[27]W. Pötz and P. Vogl, Phys. Rev. B **24**, 2025 (1981).

[28]The influence of the relativistic effects on the bonding properties in lead is examined in more detail in N. E. Christensen, S. Satpathy, and Z. Pawloska, Phys. Rev. B **34**, 5977 (1986).

[29]L. Kleinmann, Phys. Rev. **128**, 2614 (1962).

[30]G. L. Bir and G. E. Pikus, Fiz. Tverd. Tela (Leningrad) **3**, 3050 (1961), [Sov. Phys.—Solid State **2**, 2039 (1961)].

[31]A. Blacha, H. Presting, and M. Cardona, Phys. Status Solidi. B **126**, 11 (1984).

[32]*Physics of Group IV Elements and II-V Compounds,* Vol. 17, Teil a of Landolt-Börnstein (Springer-Verlag, Heidelberg, 1982).

[33]N. E. Christensen, Solid State Commun. **50**, 117 (1984); Phys. Status Solidi B **123**, 281 (1984); Phys. Rev. B **30**, 5753 (1984).

[34]O. H. Nielsen and R. M. Martin, Phys. Rev. Lett. **50**, 697 (1983); Phys. Rev. B **32**, 3792 (1985); O. H. Nielsen, *ibid.* **34**, 5808 (1986).

[35]P. N. Keating, Phys. Rev. **145**, 637 (1966).

[36]R. M. Martin, Phys. Rev. B **1**, 4005 (1970).

[37]These potentials introduce artificial Darwin shifts of the $s$ states. A more detailed account is given in N. E. Christensen, Phys. Rev. B **30**, 5753 (1984).

[38]O. H. Nielsen, Phys. Rev. B **34**, 5808 (1986).

[39]The FPM expression (52) assumes that the band structure is calculated (within the density-functional formalism) self-consistently for one structure (I). The potentials generated are then moved to the new atomic positions, structure II. Then one, single-band calculation is performed. The charges $q_{RII}$, from this calculation are used in $\Delta E^{\mathrm{STR}}_{\mathrm{Madelung}}$, and $\Delta \sum_i \varepsilon_i$ is the difference in the sum of one electron energies from the last (non-self-consistent) calculation and that from the first (self-consistent) calculation. We have here (and in Ref. 1) iterated to self-consistency in the $B3$ structure. In the present calculations we use the crudest approximation, the ASA (atomic spheres approximation) to the total energy difference Eq. (52). The so-called "combined correction term" (Ref. 18) is included in the calculation of the one-electron energy sum.